https://doi.org/10.5194/egusphere-2026-4710
Preprint. Discussion started: 18 August 2026

Reduction and evaluation of a near-explicit dimethyl sulfide and methanethiol oxidation mechanism

Lorrie S. D. Jacob[1], Yao Ge[1], Chiara Giorio[1], and Alexander T. Archibald[1,2]

[1]Yusuf Hamied Department of Chemistry, University of Cambridge, Cambridge, CB2 1EW, UK
[2]National Centre for Atmospheric Science, Cambridge, CB2 1EW, UK

Correspondence: Lorrie S. D. Jacob (lj384@cam.ac.uk) and Alexander T. Archibald (ata27@cam.ac.uk)

Abstract.

Marine sulfur species play a key role in the Earth system, but simulating their complex oxidation mechanisms is a significant challenge for Earth system models. We have taken a comprehensive gas-phase mechanism of the OH and NO_3-initiated oxidation of dimethyl sulfide and methanethiol (156 reactions and 55 sulfur species) and generated a series of reduced complexity mechanisms using an automated rates-based approach for future incorporation into global models. Four reduced mechanisms were produced, ranging from 38–91 reactions. While the error in the reduced mechanisms typically increased with fewer reactions, the smallest mechanism, which included 38 reactions and 18 species, had an average error of less than 15% in the concentrations of key sulfur species compared to the full mechanism. This reduced mechanism was compared to a published mechanism of similar size (38 reactions) used in global modelling, which showed average concentrations of methanesulfonic acid and OCS differed by factors of 15 and 3.6, respectively, across all marine box models. While the most reduced mechanism constitutes a large increase in the number of reactions and species typically used in Earth system models for dimethyl sulfide and methanethiol, it provides a traceable link to the most recent experimental work on the subject. To assess its performance in a global modelling framework, an adapted reduced mechanism from this work was implemented into UKCA/UKESM, where it outperformed the highly simplified StratTrop dimethyl sulfide oxidation mechanism when evaluated against ATom-3 and ATom-4 measurements.

1 Introduction

Dimethyl sulfide (CH_3SCH_3, DMS) is the largest natural source of sulfur in the atmosphere, with around 28 Tg S emitted annually from phytoplankton (Lana et al., 2011). Additionally, methanethiol (CH_3SH, MeSH) has recently been found as another large source of sulfur in the atmosphere, with emissions around 15–40% of DMS emissions (Wohl et al., 2024). The products of both DMS and CH_3SH include sulfuric acid (H_2SO_4, SA) and methanesulfonic acid (CH_3SO_3H, MSA), species known to contribute to cloud condensation nuclei (Curry and Webster, 1999; Boy et al., 2005; Kulmala, 2003), and new particle formation (Kerminen et al., 2018; Covert et al., 1992; Beck et al., 2021; Baalbaki et al., 2026). DMS chemistry affects indirect radiative forcing, which in turn will affect the modelling of global climate and predictions of future climate scenarios (Fung

https://doi.org/10.5194/egusphere-2026-4710
Preprint. Discussion started: 18 August 2026

et al., 2022; Szopa et al., 2021). As such, an accurate representation of DMS oxidation in Earth system models is needed to improve their modelling of Earth's radiative balance, and subsequently, predictions of global average temperatures.

Following the recent rejuvenation of interest in volatile sulfur chemistry after the discovery of hydroperoxymethyl thioformate ($OCHSCH_2OOH$, HPMTF, Veres et al. (2020)), and large emissions of CH_3SH (Wohl et al., 2024), several studies have revised the treatment of DMS and CH_3SH, incorporating updated reactions and rate constants from experimental and theoretical studies into global chemical transport models such as GEOS-Chem (Chen et al., 2023; Tashmim et al., 2024) and COSMO-MUSCAT (Hoffmann et al., 2020), and Earth system models such as UKCA/UKESM (Cala et al., 2023) and CAM6-Chem/CESM2 (Fung et al., 2022). These DMS oxidation mechanisms have not undergone evaluation using chamber studies, as done with the mechanism from Jacob et al. (2024), or an assessment of their uncertainty as in Jacob et al. (2026). Only the mechanism by Hoffmann et al. (2020) is based on a larger, near-explicit mechanism, however, that mechanism does not include the HPMTF pathway. Intercomparisons of some of these mechanisms demonstrated the sensitivity of the global models to the DMS oxidation mechanism used, and comparison with observations showed that the mechanisms were unable to reproduce observed concentrations of DMS oxidation products (Cala et al., 2023; Jongebloed et al., 2025). The development of a DMS mechanism for use in global models that is made systematically and includes updates from the recent literature is required to improve the representation of DMS in global models.

Running Earth system models and global chemical transport models is computationally expensive, and, in the case of the Met Office UM-UKCA model, the chemistry and photolysis component can be responsible for 10-20% of the total run time (Esentürk et al., 2018). As such, the chemical mechanisms included in these models are simplified; DMS oxidation mechanisms used in these models that incorporate HPMTF chemistry, along with more complicated CH_3SO_x chemistry, include around 40 reactions (Tashmim et al., 2024; Chen et al., 2023; Cala et al., 2023). Ideally, the evaluated mechanism developed in Jacob et al. (2024) and Jacob et al. (2026) should be used in global models, however, the full mechanism (containing around 160 reactions) is prohibitive for long simulations and must first be reduced.

A range of reduction methodologies have been used in the literature (Ervens et al., 2024), with the approach depending on the size of the original mechanism and its application. Reduction methods can range from more computationally expensive methods such as the Morris method (Chang et al., 2020), to faster methods utilising graph theory (Wiser et al., 2023). In addition to the method of reduction, the environmental and chemical parameters used to apply the method will affect the applicability of the reduced mechanism. Using a small sample space such as a chamber study can bias the final mechanism; Jacob et al. (2024) showed that mechanisms optimised to one chamber did not perform well against data from a different chamber. There is no perfect reduction methodology, and while highly reduced mechanisms can be made, they may result in the use of representative intermediates that do not have physical analogues. Furthermore, Earth system models often do not have any formal mechanism reduction strategy, and more work is needed to ensure that the chemistry utilised by those models represents our current understanding.

A sensitivity analysis such as the Morris method provides an effective way to rank reactions based on the sensitivity of a modelled output, and this ranking can be used to produce reduced mechanisms (Chang et al., 2020). However, sensitivity analysis requires hundreds or thousands of simulations for each set of conditions analysed (usually via a box model), with the

https://doi.org/10.5194/egusphere-2026-4710
Preprint. Discussion started: 18 August 2026

result only applicable to those conditions (Stein et al., 2022). The marine atmosphere covers a large range of meteorological conditions and oxidant concentrations, selecting only a few locations to perform a sensitivity analysis could result in a bias in the reduced model.

Reduction methods based on the rates of each reaction in a box model can successfully create reduced mechanisms by using only one simulation for each chemical regime; the concentrations of key species from the reduced mechanisms typically differ by only 2.5–5% from the full mechanisms under the modelled conditions (Ervens et al., 2003; Mauersberger, 2005; Deguillaume et al., 2009; Hoffmann et al., 2020). These methods compare the contribution of different reactions to the total chemical formation (or loss) of a species against a threshold yield to determine which reactions should be included in the reduced mechanism.

Recently, graph theory has been used in the reduction of the isoprene oxidation mechanism to create the AMORE-Isoprene mechanism, without the use of box models. Although this method managed to reduce the complexity of a large mechanism, the reduced mechanism required manual input as it led to surrogate species that have no physical analogues (Wiser et al., 2023). While the use of graph theory in mechanism reduction still requires improvement, a rates-based reduction method provides a traceable, reliable methodology that is not computationally expensive.

Following the reduction of a larger reference mechanism, the resulting mechanism must be evaluated against the reference mechanism, however, this process of evaluation differs between studies (Hoffmann et al., 2020; Jenkin et al., 2019; Squire et al., 2015; Wang et al., 2022). In some cases, the reduced mechanisms have been evaluated using a few box models representing different environmental conditions, as was the case for the reduced Chemical Aqueous Phase Radical Mechanism (CAPRAM) DMS oxidation mechanism by Hoffmann et al. (2020), which was compared to three box models at a single latitude. However, these models are not likely to represent all marine environments where DMS oxidation occurs. Similarly, with respect to isoprene oxidation, the Common Representative Intermediates (CRI) was developed and evaluated using a single tropical forested boundary layer box model, with the mixing ratio of NO_x and volatile organic compounds adjusted in different runs (Jenkin et al., 2015, 2019). This variation in parameter space was further expanded to generate isopleths, which have also been used to evaluate reduced mechanisms by comparing the performance of the reduced mechanism to the reference mechanism using a series of box models (Squire et al., 2015). The use of isopleths is limited unless the influence of additional parameters are explored. These evaluation frameworks do not explore different temperatures or photolysis rates, which will impact the oxidation of the species of interest; Archibald et al. (2020b) showed changes in temperatures lead to significant variation in mechanisms used in global models. Alternatively, Wang et al. (2022) evaluated their reduced mechanism using around 12'000 box models across continental Europe spanning 12 months, based on results from a global chemical transport model. This methodology (using randomised box models developed using global modelling results) provides a thorough evaluation framework, which ensures that all relevant environmental conditions are explored, and increases the reliability of the reduced mechanism.

In this work, we reduced the mechanism developed in Jacob et al. (2024), and updated in Jacob et al. (2026), through an automated rates-based approach, similar to the method used by Hoffmann et al. (2020) in their reduction of the DMS mechanism. To reduce the mechanism, one hundred box models of the marine boundary layer were used. These models were

https://doi.org/10.5194/egusphere-2026-4710
Preprint. Discussion started: 18 August 2026

randomly sampled across time and space, and based on a reanalysis of meteorological data (ERA5) and the concentrations of species from an Earth system model (UKCA/UKESM). Mechanisms of different sizes were created, and their performance was evaluated against the full mechanism using one thousand randomised box models of the marine boundary layer, in a similar approach as Wang et al. (2022).

2 Randomised marine boundary layer box models

The reduction and evaluation of the reduced mechanisms have been performed using randomised box models of the marine boundary layer based on hourly ECMWF Reanalysis v5 (ERA5) data (Hersbach et al., 2023) and monthly UK Earth System Model (UKESM) modelled surface concentrations of species used to constrain the box model, covering the period from 1st October 2013 to 30th September 2014.

The United Kingdom Chemistry and Aerosol (UKCA) model, the chemistry-aerosol component of UKESM, was employed in an atmosphere-only (AMIP) configuration using version 13.5. Simulations were performed at a horizontal resolution of 1.25° × 1.875° with 85 vertical levels extending up to 85 km (Walters et al., 2019). A 14-month simulation period was used, from August 2013 to October 2014, with the initial two months designated as spin-up. Meteorological fields, including temperature, pressure, precipitation, and wind, were nudged to ERA5. UKCA incorporates the GLOMAP-mode aerosol scheme (Mann et al., 2010), which simulates size-resolved aerosol microphysics (nucleation, condensation, coagulation, and cloud processing). This scheme transports the mass of sulfate, ammonium, nitrate, sea salt, black carbon, organic matter, and dust, as well as the particle number concentration for each size mode. Oceanic emissions of DMS and CH_3SH used in UKCA are based on global climatology emissions derived from Wohl et al. (Wohl et al., 2024). The chemistry scheme employed is the standard StratTrop mechanism (Archibald et al., 2020a), augmented by an additional set of DMS and CH_3SH oxidation reactions, from a preliminary reduced DMS mechanism based on Jacob et al. (2024).

Between the available dates, the modelled days (based on UTC time) were randomly chosen based on a uniform distribution (i.e. each day had equal weighting). Independently, latitude and longitude were randomly sampled, with longitude also sampled using a uniform distribution. To ensure uniform sampling across the Earth, latitude was sampled using the sphere point-picking method from Weisstein (2002). Specifically, a polar angle was calculated using

$$\phi = \cos^{-1}(2v - 1)$$

where v was randomly chosen from a uniform distribution between 0 and 1. The polar angle, ϕ, was then converted to latitude. If latitude had also been randomly sampled using a uniform distribution, the poles would be oversampled, as the circumference of a latitude line is smaller in the polar regions compared to the tropics (Weisstein, 2002).

If the latitude and longitude coordinates found using the above method were over land, they were rejected, and new co-ordinates were chosen at the same time point. Each randomly sampled time, latitude and longitude were then compared to the closest available ERA5 and UKCA grid points at the surface. If the coordinates at the time chosen were over sea ice, as determined by ERA5 data, they were also rejected. Finally, if the monthly mixing ratio of NO_2 (determined from UKCA data)

https://doi.org/10.5194/egusphere-2026-4710
Preprint. Discussion started: 18 August 2026

was higher than 2 ppbv, the coordinates were rejected. The threshold (2 ppbv of NO_2) was chosen as it represents the 99th percentile of monthly average surface concentrations from UKCA over the ocean (depicted in Figure S1). These tests ensure the sampled box models were over the ocean and not in highly polluted environments.

Figure 1 shows the thousand points used for the evaluation of the reduced mechanism (dark blue), the hundred points used for the reduction (orange), and the points rejected due to NO_2 mixing ratios higher than 2 ppbv (red). Once the coordinates and time points for the box models were chosen, ERA5 and UKCA data were used to build the box models.

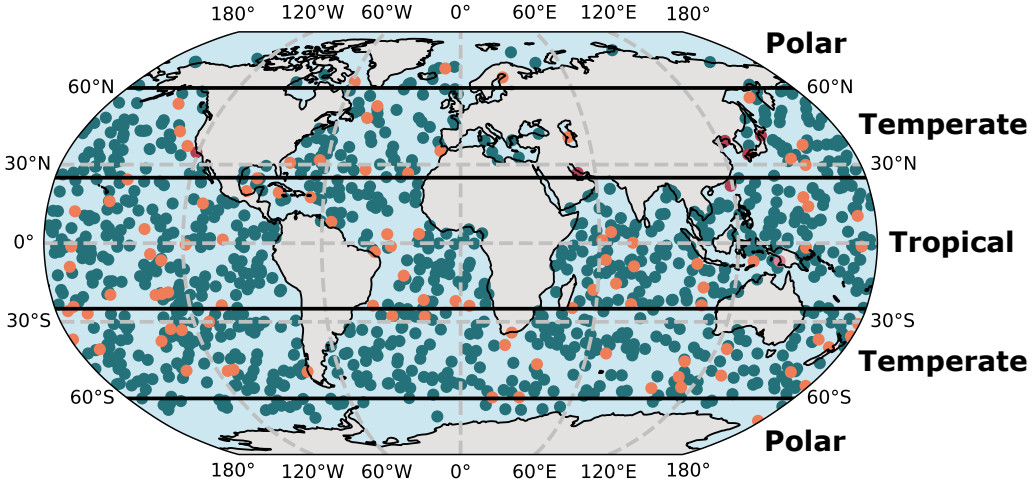

Figure 1. The randomly sampled locations for the evaluation (blue points), along with the samples omitted from the evaluation due to average NO_2 mixing ratios higher than 2 ppbv (red points). The locations used for the reduction are given as orange points.

As with Jacob et al. (2026), photolysis rates were calculated using zenith angles based on the latitude, longitude and date of the box models, and cloudless days were assumed. A constant boundary layer height of 750 m was used for all models, and the dilution of species was not included.

Hourly ERA5 data was used to determine dry deposition velocities, relative humidity, temperature, and pressure. Dry deposition velocities were calculated through the same resistance method as Jacob et al. (2026), using 10 m u and v-component of wind, along with the friction velocity from ERA5 data.

Condensation sinks were based on the relative humidity-dependent aerosol liquid water content (LWC) and pH calculated in Jacob et al. (2026) using polar, temperate and tropical fieldwork data. The coordinates of each box model were used to allocate the model into a latitude band to use the associated LWC and pH: polar (-60° to -90° and 60° to 90°), temperate (-25° to -60° and 25° to 60°) or tropical (-25° to 25°). Relative humidity from ERA5 data was used to obtain the hourly liquid water content and pH across the modelled day, which was then averaged and used in the model. A constant aerosol radius of 0.38 μm was used, based on work from Hoffmann et al. (2016) and as used in Jacob et al. (2026). The condensation sinks were calculated using the same method as Jacob et al. (2026); the condensation sinks for H_2SO_4 used in the box models are shown in Figure 2.

https://doi.org/10.5194/egusphere-2026-4710
Preprint. Discussion started: 18 August 2026

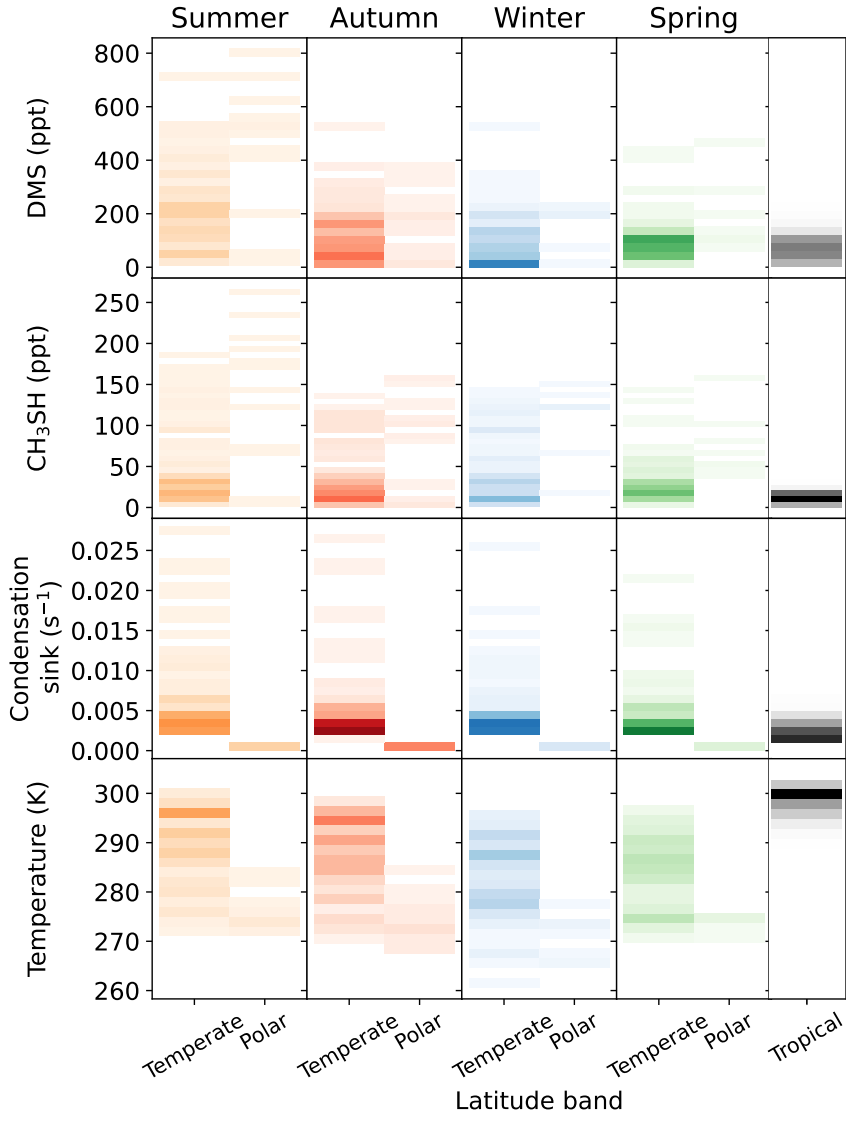

Figure 2. The mixing ratios of DMS and CH_3SH, along with the condensation sinks of H_2SO_4 and the average temperature in the 1000 marine box models, separated by seasons and latitude bands. The colour intensity represents the number of box models within each bin, with the darkest colour corresponding to 50 box models per bin. For the tropical latitude band, which represents 12 months rather than 4, the darkest colour corresponds to 200 box models per bin.

145 Monthly surface mixing ratios from UKCA were used to constrain DMS, CH_3SH, CO, O_3, NO_3, NO_2, NO, HO_2, OH and HCHO. Additionally, the annual mean mixing ratio of methane in 2014 was used, which was obtained from the National Oceanic and Atmospheric Administration (NOAA, 1822.54 ppb) (Lan et al., 2025). The concentrations of DMS, CH_3SH, O_3, CH_4, and HCHO were kept constant throughout the box model; the mixing ratios of DMS and CH_3SH used in the box models

https://doi.org/10.5194/egusphere-2026-4710
Preprint. Discussion started: 18 August 2026

are shown in Figure 2. The diurnal cycles of NO_3, NO_2, NO, HO_2 and OH were accounted for by using calculated photolysis rate constants, and scaling them to the same average mixing ratio as the UKCA output for the species of interest. This ensured that the daily average concentration of these species was the same as the UKCA output, while the hourly concentration followed a diurnal cycle similar to their concentration in the marine environment, demonstrated in Figure 3.

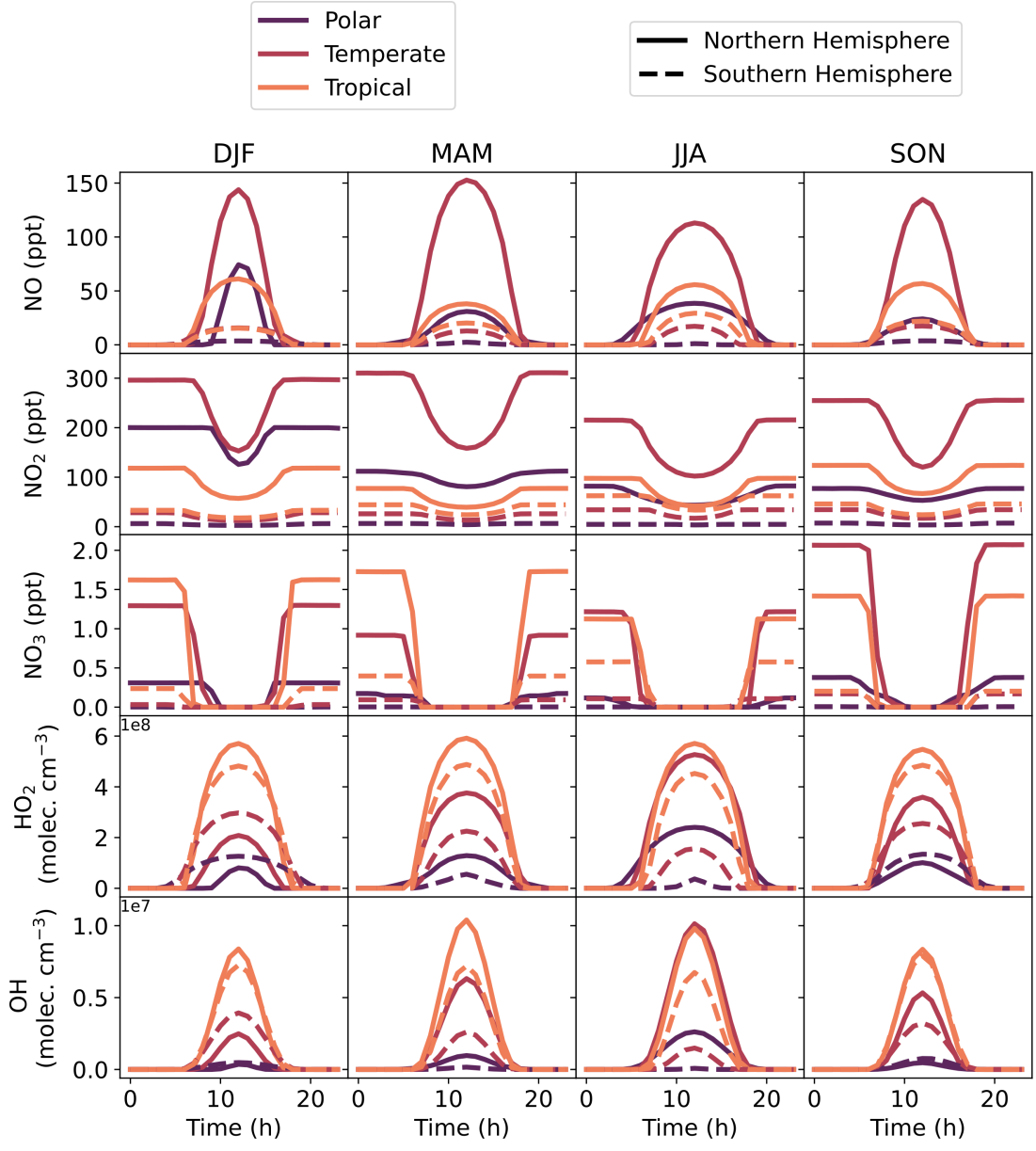

Figure 3. The average hourly input mixing ratio of NO, NO_2, and NO_3 and concentration of OH and HO_2 over different latitude bands and months for the box model simulations over the marine boundary layer.

https://doi.org/10.5194/egusphere-2026-4710
Preprint. Discussion started: 18 August 2026

Specifically, the photolysis rate constant of O_3 (forming $O(^1D)$ radicals, referred to here as J_{O_3}), was used for the diurnal cycle of OH, and the photolysis of NO_2 (forming NO, J_{NO_2}) was used for HO_2 and NO. Assuming NO_x is conserved, the concentration of NO_2 at time t was found by subtracting the previously calculated concentration of NO at time t from the average concentration of NO and NO_2,

$$[NO_2]_t = \overline{[NO_2]} + \overline{[NO]} - [NO]_t$$

The NO_3 concentration was based on the photolysis of NO_3 (forming $O(^3P)$ radicals, referred to here as J_{NO_3}), however, in contrast to OH, HO_2 and NO, the fast photolysis of NO_3 results in low mixing ratios of NO_3 in the daytime. As such, the concentration was found using the assumption that the concentration of NO_3 is zero when J_{NO_3} is larger than 0.03 s^{-1}:

$$[NO_3]_t = \overline{[NO_3]} \times \frac{x_t}{\overline{x}}$$

where

$$x_t = 0.03 - \min\{J_{NO_3,t}, 0.03\}$$

When J_{NO_3} was consistently larger than 0.03 s^{-1} (i.e. over polar summer), the concentration of NO_3 was set to the average concentration. In addition, when the $J_{H_2O_2}$, J_{O_3} or J_{NO_3} were zero throughout the full day (polar winter), the concentrations were also kept constant based on their average concentration. The average hourly concentration of NO, NO_2, NO_3, OH and HO_2 over different latitude bands and months are shown in Figure 3.

The distributions of DMS, SO_2 deposition, and J_{NO_2} from the box models were compared to the monthly surface averages over the ocean from UKCA in Figure S2. The concentration of DMS was obtained directly from UKCA, demonstrating that the sample space covered by the 1000 random box models represents the full UKCA model. Additionally, J_{NO_2} and SO_2 deposition were calculated for this work based on zenith angle and ERA5 hourly data, respectively, demonstrating that simplified zero-dimensional box models are able to replicate processes in the global model.

2.1 Dimethyl sulfide oxidation

The daily average percentage oxidation from the three pathways in each box model is shown in Figure 4; the average oxidation of DMS across all the box models for the addition of OH, H-abstraction by OH and H-abstraction by NO_3 was 28%, 43% and 28%, respectively. Similarly, Cala et al. (2023) found that 25% of global DMS oxidation occurs through reaction with NO_3 radicals, while 41% occurred through the addition of OH. Although the marine box models developed in this work use output concentrations from the same global model used by Cala et al. (2023), our box models only account for the chemistry at the surface, and utilise monthly averages. The difference between Cala et al. (2023) and this work may be attributed to the temperature dependence of the reaction with OH. At higher altitudes, the decrease in temperature would increase the rate of OH addition compared to OH H-abstraction, and increase the ratio of DMS undergoing oxidation through OH addition. However, due to its average lifetime of 1–2 days (Fung et al., 2022; Chen et al., 2018; Cala et al., 2023; Jongebloed et al., 2025), a large fraction of DMS is expected to be oxidised within the marine boundary layer before being transported to higher altitudes. As such, the set-up utilised in this work is considered representative of DMS oxidation in the marine environment.

https://doi.org/10.5194/egusphere-2026-4710
Preprint. Discussion started: 18 August 2026

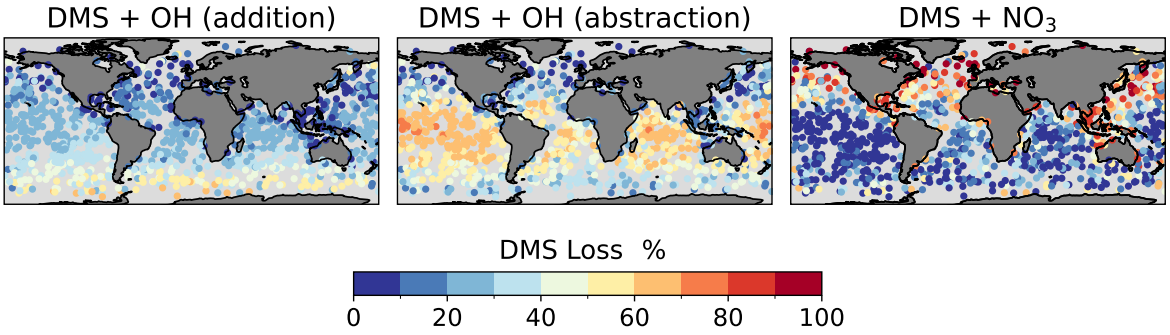

Figure 4. The DMS oxidation ratios for each location used in the 1000 box models, calculated using the dates and average monthly surface concentrations used in this work.

3 Reduction method

The reduction methodology is similar to that used by Hoffmann et al. (2020), while the evaluation, based on randomised models developed using global modelling results, resembles the work done by Wang et al. (2022). Although a sensitivity analysis, such as the Morris method, would provide a ranking of the importance of the reactions to the concentrations of different species, the analysis would require thousands of box model simulations for each marine condition chosen (Campolongo et al., 2007). To allow for more marine conditions to be considered in the reduction of the full mechanism, the reduction methodology used in this work was based on a comparison of the reaction rates, with only one box model considered for each marine condition. Our methodology is outlined as follows, with the individual steps described in more detail in the rest of this section:

1. **Run sample box models** of the marine boundary layer
2. **Calculate source and sink ratios** for each species with all related reactions
3. **Select reactions using sinks-based approach** dependent on the chosen threshold ratio
4. **Select additional reactions using sources-based approach** dependent on the chosen threshold ratio
5. **Combine reactions** of intermediate species that only have one loss pathway
6. **Evaluate reduced mechanism** by comparing to independent randomised box models

3.1 Sampled box models

One hundred randomised box models of the marine boundary layer were created, using the methodology described in Section 2, with the chosen locations shown in Figure 1. The number of models used in the evaluation (one thousand) was chosen to be a factor of 10 larger, to ensure that reduction is successful over a wider range of marine conditions. Figure S2 demonstrates that these 1000 box models are able to represent the distribution of UKCA data.

https://doi.org/10.5194/egusphere-2026-4710
Preprint. Discussion started: 18 August 2026

3.2 Calculation of source and sink ratios

For each box model, the temperature, pressure, and concentrations of species were used to calculate the rates of all the reactions in the full DMS mechanism. The box models were run for eight days to allow a 'spin-up' period, and on the last modelled day the rates calculated at each time step (10-minute increments) for each reaction were integrated to provide the total loss or formation of a species from that reaction over one day. For each species, the reactions involved in the loss of that species were expressed as a fraction of the total chemical loss for that species (sink ratio). In the example depicted in Figure 5, the sink ratio of a reaction is equivalent to the ratio between cumulative loss from that reaction and the total cumulative loss for DMS at the end of the day. For this example, the sink ratios for OH abstraction, OH addition, and reaction with NO_3 are 32%, 49%, and 18%, respectively. The same method was used with the formation of a species from different reactions to provide source ratios.

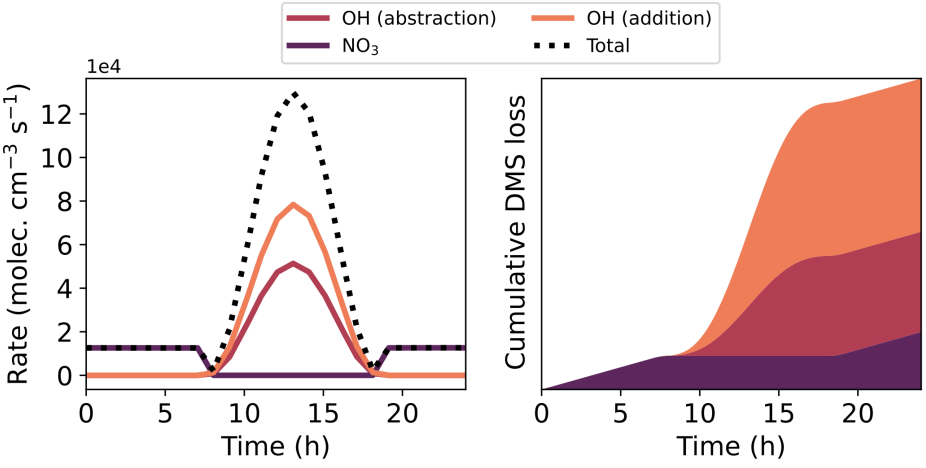

Figure 5. The DMS oxidation rates from the major reaction pathways over the final modelled day for a randomly selected box model, along with the cumulative DMS loss from those reactions across that same period.

For reversible reactions, the total loss of the product, excluding the reverse reaction, was used to determine the net loss of the reactant through the equilibrium reaction. For example, for the reaction of CH_3SO_2 with oxygen forming $CH_3SO_2O_2$, the net loss is dependent on the equilibrium rate constant, and the reactions of CH_3SO_2 and $CH_3SO_2O_2$. The effective loss of CH_3SO_2 through the reaction with oxygen was determined by combining the rates of reactions of $CH_3SO_2O_2$ (such as reactions with HO_2 or RO_2), while excluding the reaction that regenerated CH_3SO_2.

3.3 Sinks-based approach

Once the sink ratios for each species have been obtained over all one hundred box models, they were averaged and used for the initial selection of species and reactions in the reduction. Figure 6 shows the distribution of sink ratios for the major oxidation pathways of DMS included in the 1000 box models. The equivalent figure for the 100 box models used in the reduction is

https://doi.org/10.5194/egusphere-2026-4710
Preprint. Discussion started: 18 August 2026

provided in the supplementary (Figure S3) while the larger sample size is shown here to better illustrate the distributions. The mean sink ratio and 95th percentile for each distribution are also indicated.

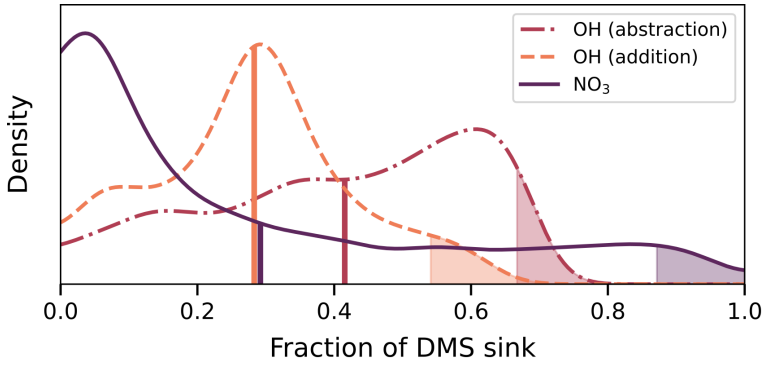

Figure 6. The distribution of the sink ratios calculated for DMS across the 1000 randomised box models of the marine surface atmosphere. The coloured vertical lines indicate the mean sink ratio for each pathway, while the shaded region represents values above the 95th percentile (i.e. the highest 5% of sink ratio values). For clarity, the minor oxidation pathways of DMS (oxidation via $O(^3P)$ and CH_3SO_3) have been excluded.

The sinks-based approach, demonstrated in Figure 7, begins with the chosen initial species: for this work, these initial species are DMS and CH_3SH. A threshold ratio is also decided, which will determine the size of the reduced mechanism, along with its performance. In the example demonstrated in Figure 7, a threshold of 30% was chosen.

Starting with DMS and CH_3SH, any reaction involved in their loss that had a larger sink ratio than the threshold was included in the reduced mechanism, along with the products of that reaction. The reactions of those products were also included if they surpassed the threshold ratio. This process continued for all products that were subsequently included.

To account for outliers (e.g. coastal regions with elevated NO_x) an additional metric was included. For one reaction, if the sink ratio at the 95th percentile was over double the threshold, that reaction was included in the reduced mechanism. Using the 30% threshold as an example, the addition reaction of DMS and OH and the reaction of DMS and NO_3 would initially be excluded from the reduced mechanism, as their average sink ratios (28% in both cases) are below 30%. However, with the additional metric, the reaction of DMS and NO_3 would be retained, as the 95th percentile (87%, see Figure 6) is larger than double the threshold (60%).

3.4 Sources-based approach

Although the sinks-based approach provides a reduced mechanism that can be used without further additions, depending on the threshold ratio chosen the production of minor, but atmospherically important, products could have been excluded. In this work, methanesulfonic acid (CH_3SO_3H, MSA) and OCS were chosen as products to include in the reduced mechanism through the sources-based approach.

https://doi.org/10.5194/egusphere-2026-4710
Preprint. Discussion started: 18 August 2026

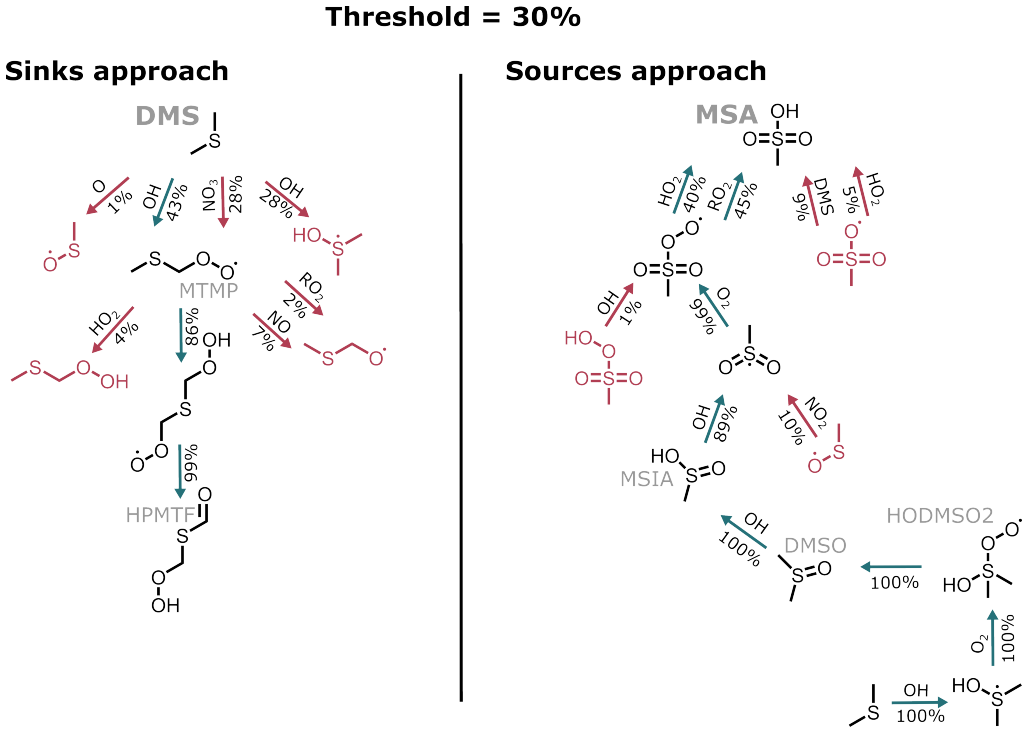

Figure 7. A depiction of the sinks-based reduction approach using DMS as the starting species, along with the sources-based reduction starting with methanesulfonic acid. The threshold ratio in this example is 30%, with blue lines indicating reactions that pass this threshold, and red lines indicating reactions that do not. For illustrative purposes, the sinks-based approach example has stopped at HPMTF.

The reactions forming the initial product, such as MSA, whose source ratios surpassed the threshold ratio were included in the reduced mechanism, along with the precursor species involved in that reaction. The major reactions forming those species (based on the threshold ratio) were also included, along with the reactants from those reactions, and so on. Similarly to the sinks-based approach, reactions with a source ratio at the 95th percentile larger than double the threshold were included.

Any species that had been included through the sources-based approach underwent the sinks-based approach to ensure that their major loss pathways had also been included.

3.5 Combining reactions

Finally, some reactions were combined to reduce the mechanism further. Depending on the threshold ratio used, for some species only one loss reaction was included in the mechanism. If that species was a short-lived intermediate, the intermediate species was removed, and the products from its loss pathway were included in the formation reaction; the rate constant used for the combined reaction was the rate constant from the formation reaction. For example, the sole reaction of CH_3SCH_2O (a product of CH_3SCH_2OO reactions) is decomposition. To reduce the total number of reactions in the reduced mechanism, CH_3SCH_2O was not included in the mechanism, and its decomposition was incorporated into its formation reaction. This

https://doi.org/10.5194/egusphere-2026-4710
Preprint. Discussion started: 18 August 2026

meant that in the reduced mechanism, these two reactions

$CH_3SCH_2OO + NO \xrightarrow{k_1} CH_3SCH_2O + NO_2$

$CH_3SCH_2O \xrightarrow{k_2} CH_3S + HCHO$

were combined into one:

$CH_3SCH_2OO + NO \xrightarrow{k_1} CH_3S + HCHO + NO_2$

3.6 Evaluating the reduced mechanism

In this work, the performance of the reduced mechanism was evaluated against the full mechanism, using one thousand randomised box models of the marine boundary layer. The normalised mean bias (NMB) over the final model day was considered, with NMB_i, the bias of a species i due to the reduction of the mechanism, calculated as

$$NMB_i = 100\% \times \frac{\sum_{t=0}^{N}(R_{i,t} - F_{i,t})}{\sum_{t=0}^{N} F_{i,t}} \quad (1)$$

where $R_{i,t}$ and $F_{i,t}$ are the concentrations of species i at time t from the reduced and full mechanisms, respectively. For species such as MSA and sulfuric acid, concentrations approach zero during the nighttime hours; calculating a relative bias using their instantaneous concentration can result in artificially large biases despite the absolute differences being small. Therefore, evaluation metrics were calculated relative to the concentration of each species over the 24 hours of the final modelled day, avoiding disproportionate weighting of periods with negligible concentrations.

The normalised mean absolute error (NMAE) was calculated using a similar method and given as a percentage. $NMAE_i$, the error of species i due to the mechanism reduction, was defined as

$$NMAE_i = 100\% \times \frac{\sum_{t=0}^{N}|R_{i,t} - F_{i,t}|}{\sum_{t=0}^{N} F_{i,t}} \quad (2)$$

Using these metrics, an error or bias of zero indicates that the reduced mechanism outputs the same concentration as the full mechanism for species i.

4 Gas-phase dimethyl sulfide and methanethiol mechanism

The full mechanism used in this reduction work was the updated gas-phase DMS oxidation mechanism from Jacob et al. (2026), along with CH_3SH oxidation through reactions with OH and NO_3. Halogen and aqueous chemistry were not included as the concentrations of the gas-phase halogen species or aqueous oxidants (in aerosols), which are needed for those reactions, were not provided through the UKCA data. However, halogen reactions have been found to be important oxidation reactions for DMS (Hoffmann et al., 2016; Chen et al., 2018), and these reactions can be subsequently added to the reduced mechanism, as described in Section 6. The uncertainties in the full mechanism, based on known gas-phase chemistry, have been explored in Jacob et al. (2026), with uncertainties in the concentration ranging from 10–200% for most species. The aim here is not to

https://doi.org/10.5194/egusphere-2026-4710
Preprint. Discussion started: 18 August 2026

propagate those uncertainties further, but to develop a framework that enables the generation of a reduced complexity scheme from a reference mechanism.

The modelled mixing ratios of major DMS and CH_3SH oxidation products for two randomly chosen marine box models are provided in Figure 8. As demonstrated by the figure, most species tended to reach steady state after a few days, with the exception of OCS, which has a global atmospheric lifetime of around six years (Seinfeld and Pandis, 2006). The last day (day eight) of the model simulations was used in the subsequent evaluation of the reduced mechanisms to approximate steady-state concentrations.

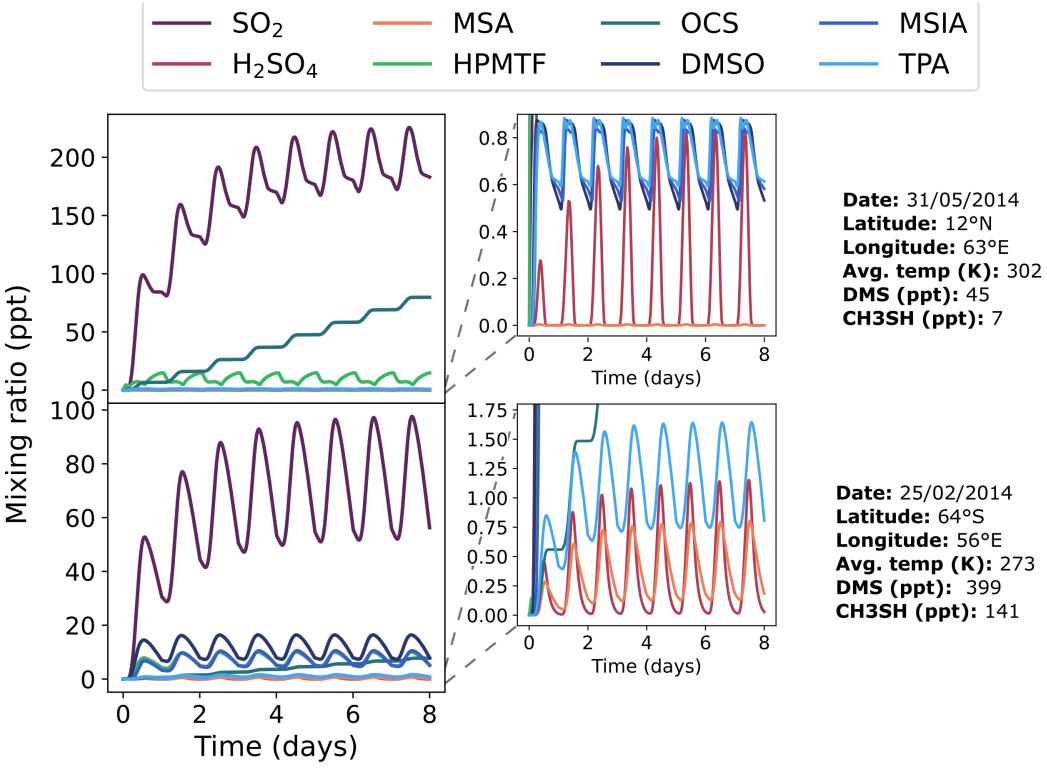

Figure 8. Two randomly chosen marine box models showing the mixing ratio of DMS and CH_3SH oxidation products over the eight-day run (first column). Information for each model is given on the right-hand side, with the second column zooming in on the y-axis to better show the mixing ratios of MSA and H_2SO_4 in those models.

5 Reduced mechanisms

Using the reduction methodology described in Section 3, four reduced mechanisms were produced, referred hereafter as mechanisms R01, R05, R10, R20, representing reductions based on thresholds of 1%, 5%, 10% and 20%, respectively. The number

https://doi.org/10.5194/egusphere-2026-4710
Preprint. Discussion started: 18 August 2026

of reactions and species in each mechanism can be found in Table 1. The reactions and species of mechanism R20 are depicted in Figure 9 and provided in the appendix (Table A1).

Table 1. A summary of the four reduced mechanisms produced in this work.

	Original mech.	R01	R05	R10	R20
Reactions	156	91	64	55	38
Species	55	33	27	24	18

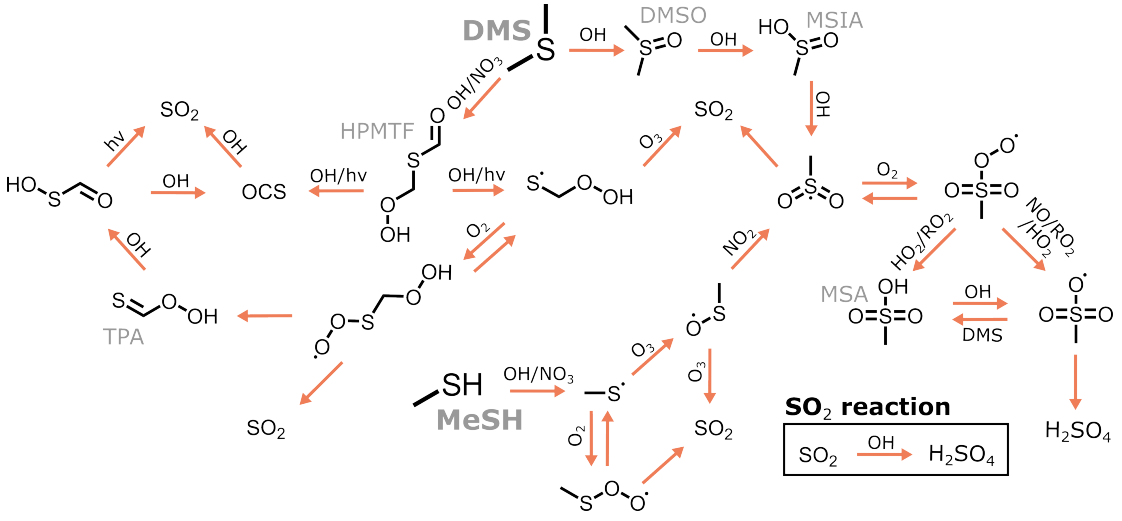

Figure 9. A schematic of the final reduced DMS and CH_3SH mechanism, R20, recommended for global modelling. Only sulfur compounds are included in this schematic for simplicity.

Additionally, a mechanism based on R20 and adapted for use in the United Kingdom Chemistry and Aerosol (UKCA) model was compared to the full mechanism in the subsequent sections. This mechanism, referred to here as 'RUKCA', contains 47 reactions and differs from R20 by including reactions of the methylthiomethyl peroxy radical (CH_3SCH_2OO, MTMP) such as the reactions with HO_2 and NO, the major reaction with RO_2, and the isomerisation into $HOOCH_2SCH_2O_2$ (which undergoes an isomerisation to form HPMTF). In R20, HPMTF is formed directly instead of CH_3SCH_2OO, which leads to larger errors in the concentration of HPMTF. RUKCA uses updated HPMTF photolysis based on the absorption cross-section calculated in Christensen et al. (2026), and removes the ROOH photolysis pathway for HPMTF based on the results from the same paper. Finally, RUKCA includes the reaction of TPA with OH forming OCS, which is omitted in R20, and includes a reaction of CH_3SO_3 with CH_3SH, forming MSA.

https://doi.org/10.5194/egusphere-2026-4710
Preprint. Discussion started: 18 August 2026

5.1 Evaluation against full mechanism

Figure 10 shows the normalised mean bias in the output concentration of different species for the reduced mechanisms when compared to the reference mechanism (due to the threshold ratio chosen). A figure showing the normalised mean absolute error in the concentrations, along with a table providing the average error and bias (and their 90% confidence interval), for each mechanism can be found in the supplementary (Figure S4 and Table S1). Mechanism R20 contains the fewest reactions and has the largest average errors for the species considered in this evaluation, which were SO_2, MSA, HPMTF, OCS, dimethyl sulfoxide (CH_3SOCH_3, DMSO), H_2SO_4 and methanesulfinic acid (CH_3SO_2H, MSIA). For these species, the average error from R20 is less than 8.1%, with the exception of OCS and HPMTF, which had an average error of 11.6% and 14.7%, respectively.

Although the average error in SO_2 increases with increasing threshold ratios (from 0.0% with the R01 mechanism, to 8.1% with R20), for some species the error does not increase considerably as the mechanism is reduced further. For example, DMSO has an average error of 0.0% for R01 which increases to 5.8% with R05, however, it only increases to 6.1% with R20. Similarly, the average error for MSIA ranges from 2.3–3.2% for all mechanisms. Figure 11 shows the normalised mean absolute error (NMAE) in DMSO from mechanism R20 (which is similar to the error from R05 and R10) as a function of temperature, and the percentage of DMS oxidation that occurs through reaction with NO_3. In the marine box models where the mechanism shows the largest error in DMSO concentration, oxidation of DMS predominantly occurs through reaction with NO_3, especially at higher temperatures. The larger error in the environments with elevated NO_x is due to the omission of the reaction of DMSO and NO_3, forming dimethyl sulfone ($CH_3SO_2CH_3$, DMSO2). The error in MSIA (the product of the reaction between OH and DMSO) is also larger in box models with higher concentrations of NO_3 and at higher temperatures. This larger error in those conditions is due to the omission of the reaction of NO_3 with both DMSO and MSIA in the reduced mechanisms. As the formation of DMSO, and subsequently MSIA, in the full mechanism occurs via the addition of OH to DMS, in the high-NO_x environments where these larger errors occur the fraction of DMSO and MSIA formed from DMS oxidation is lower.

The average bias in HPMTF increased from 4.1% to 14.7% between mechanisms R10 and R20, which is due to the removal of reactions of the methylthiomethyl peroxy radical (CH_3SCH_2OO, MTMP). In R20, CH_3SCH_2OO solely undergoes isomerisation to form the HPMTF precursor, $HOOCH_2SCH_2O_2$, however, in R10, CH_3SCH_2OO can react with NO and RO_2. Removing those reactions results in a higher concentration of HPMTF, which also increases the formation of OCS.

The error in MSA concentration from R20 correlated with both temperature and the average mixing ratio of NO, as shown in Figure 11. This relationship was also observed in mechanism R10, which is associated with the removal of the reaction between CH_3SO_3 and HO_2, forming MSA. The temperature dependence of the error arises from the thermal decomposition of CH_3SO_3; at higher temperatures, the radical is more likely to decompose into SO_3 and CH_3, making the reaction with HO_2 less important. The relationship with NO is due to the reaction between $CH_3SO_2O_2$ and NO, which forms CH_3SO_3.

Although the RUKCA mechanism is based on R20, the adjustments to the mechanism result in the differences shown in Figure 10. Notably, the reintroduction of the reactions of CH_3SCH_2OO reduces the error in HPMTF, SO_2, and H_2SO_4. However, the removal of the photolysis of the ROOH functional group in HPMTF (forming OCS), results in less OCS forming

https://doi.org/10.5194/egusphere-2026-4710
Preprint. Discussion started: 18 August 2026

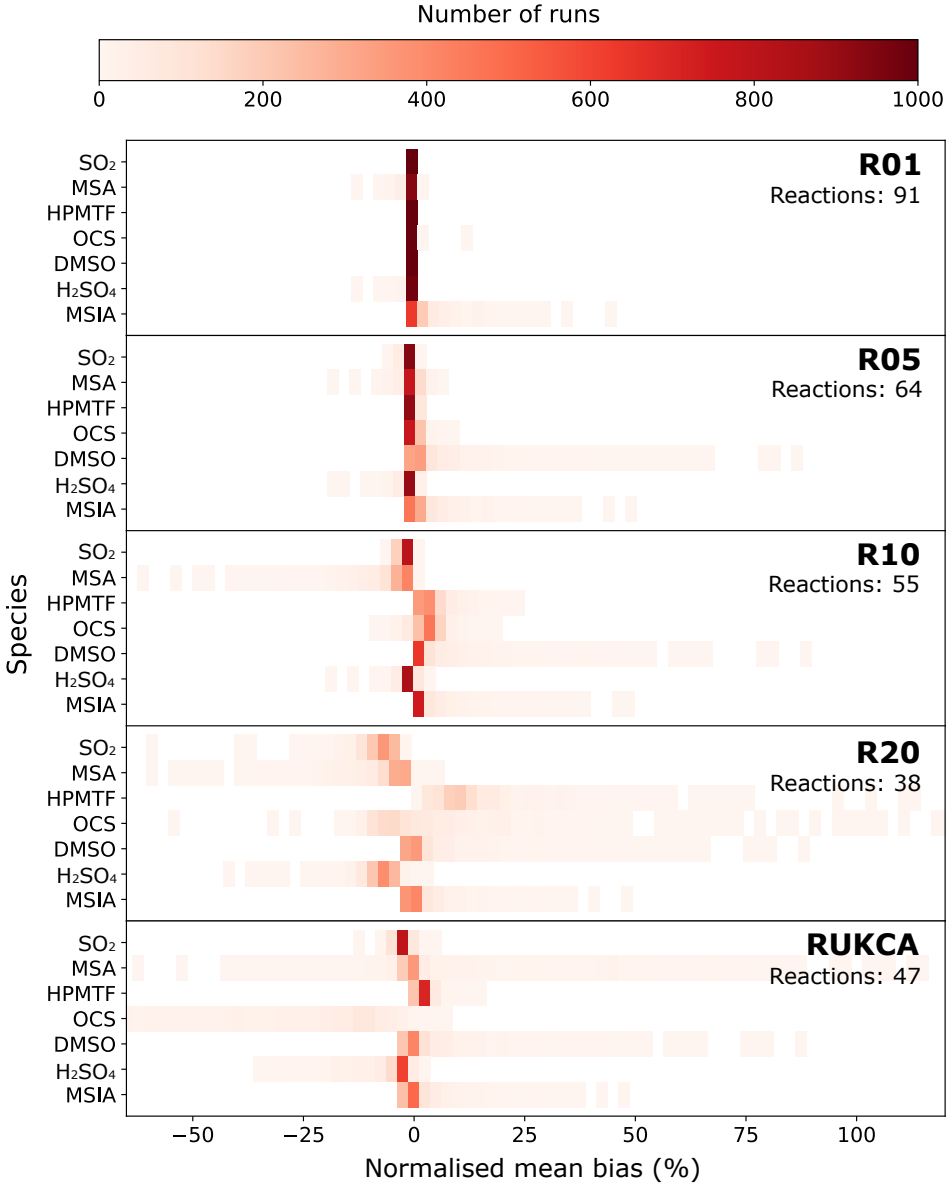

Figure 10. A heatmap of the normalised mean bias of SO_2, MSA, HPMTF, OCS, DMSO, H_2SO_4 and MSIA from the reduced mechanisms evaluated against the full mechanism for one thousand marine box models, using a bin size of 2.5%.

compared to the full mechanism, as expected. Additionally, the inclusion of the reaction between CH_3SO_3 and CH_3SH results in greater concentrations of MSA compared to the full mechanism. The differences in the concentrations of MSA and OCS in RUKCA reflect an update to the mechanism, instead of errors due to the reduction.

https://doi.org/10.5194/egusphere-2026-4710
Preprint. Discussion started: 18 August 2026

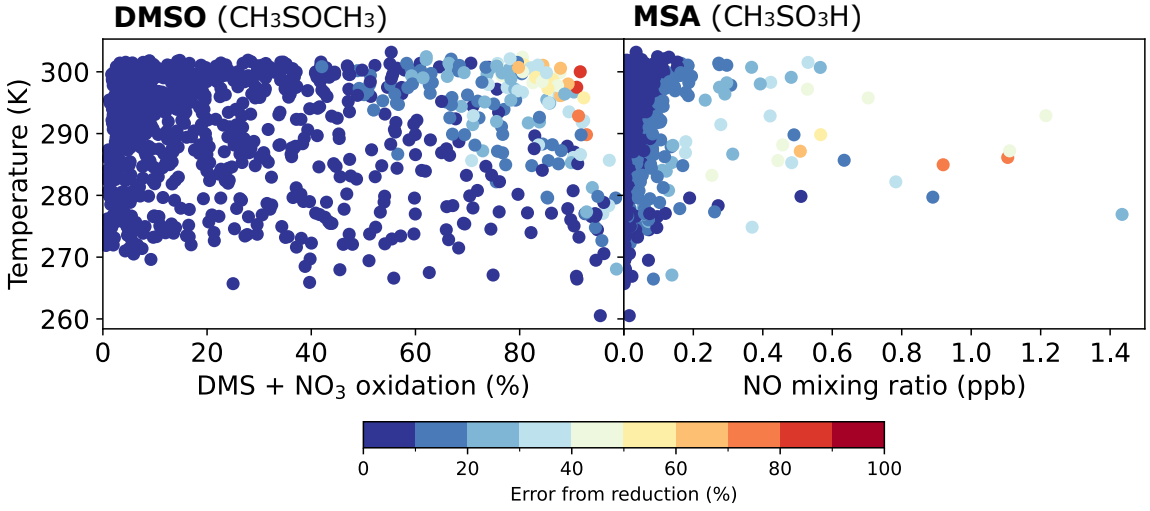

Figure 11. The percentage normalised mean absolute error in DMSO and MSA from the R20 mechanism, evaluated using the full mechanism.

5.2 Comparison with another mechanism

In addition to running the one thousand marine box models with the full and reduced mechanisms, the DMS oxidation mechanism from Cala et al. (2023) was run, hereafter referred to as the Cala mechanism. For this comparison, the condensation sinks and non-sulfur chemistry used for the other mechanisms were also used for the Cala mechanism. The Cala mechanism, which has been evaluated against other DMS mechanisms used in global models (Cala et al., 2023; Jongebloed et al., 2025), contains 38 reactions and does not include methanethiol chemistry.

Figure 12 shows the distribution of average mixing ratios in the thousand box model simulations for the Cala mechanism, along with the full mechanism (156 reactions), R20 (38 reactions), and RUKCA (47 reactions). The distributions of HPMTF, DMSO, and H_2SO_4 are similar between the four mechanisms, with the full and reduced mechanisms (R20 and RUKCA) showing similar distributions for all species.

Across all box models, the average mixing ratio of SO_2 on the last modelled day produced by the Cala mechanism, 33 ppt, is a factor of 3 smaller than the average SO_2 from the full mechanism (110 ppt), R20 (102 ppt) and RUKCA (107 ppt). The difference is due to the inclusion of methanethiol chemistry in the mechanisms developed in this work, which is a source of SO_2. The impact of CH_3SH oxidation on SO_2 concentration is demonstrated in Figure 12, which shows SO_2 concentration from the Cala mechanism with additional CH_3SH oxidation reactions. After these reactions have been added, the Cala mechanism produces a similar distribution of SO_2 concentrations as the reference and reduced mechanisms from this work, with an average SO_2 mixing ratio of 99 ppt.

The addition of CH_3SH reactions increases the modelled concentration of gas-phase H_2SO_4 in the Cala mechanism, due to the gas-phase oxidation of SO_2. However, this increase in H_2SO_4 is not proportional to the increase in SO_2, which reveals that H_2SO_4 in the Cala mechanism is primarily formed directly through DMS oxidation (i.e. not through the subsequent oxidation

https://doi.org/10.5194/egusphere-2026-4710
Preprint. Discussion started: 18 August 2026

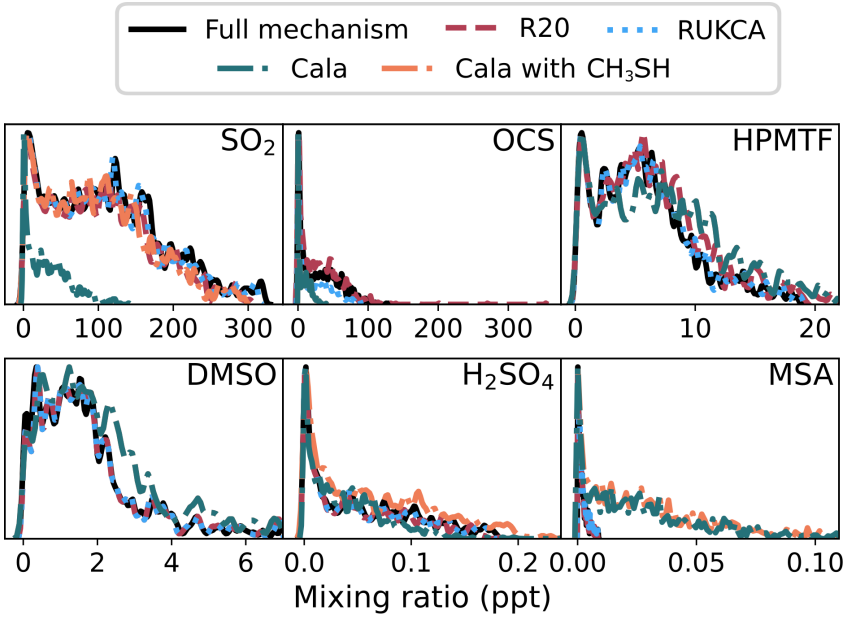

Figure 12. Density plots showing the distribution of the average gas-phase mixing ratios of SO_2, OCS, HPMTF, DMSO, H_2SO_4 and MSA on the last modelled day of the thousand marine box models using sulfur mechanisms from the full mechanism (black line), reduced mechanism R20 (red dashed line), RUKCA (blue dotted line), the mechanism developed in Cala et al. (2023) (green dot-dashed line), and the Cala mechanism with CH_3SH chemistry (Cala with CH_3SH, orange dot-dashed line).

of SO_2, but through reactions such as the decomposition of CH_3SO_3). The inclusion of CH_3SH to the Cala mechanism leads to higher concentrations of gas-phase H_2SO_4 compared to the reference and reduced mechanisms from this work; this indicates that more H_2SO_4 is formed directly from the oxidation of DMS in the Cala mechanism, compared to our mechanisms.

Additionally, the average mixing ratio of OCS from the Cala mechanism, 9 ppt, is a factor of 3.5 smaller than the full mechanism (30 ppt) and a factor of 2.8 smaller than RUKCA (24 ppt). In the Cala mechanism, OCS solely forms from the reaction of HPMTF with OH, with a branching ratio of 10%. The mechanisms developed in this work also form OCS from this pathway, with a similar branching ratio of 9%, however, the total rate constant for the reaction of OH with HPMTF is 75% larger than the rate constant used by Cala et al. (2023). Additionally, the full mechanism and R20 form OCS from another pathway; the photolysis of the ROOH group in HPMTF. This photolysis reaction is not included in RUKCA, which results in less OCS being formed.

With an average of 0.029 ppt, the Cala mechanism produces higher mixing ratios of gas-phase MSA than the other three mechanisms (0.0019–0.0021 ppt). In the mechanisms developed in this work, the equilibrium rate constant for the reaction of CH_3SO_2 with oxygen, along with the decomposition rate of CH_3SO_2, has been updated to theoretical calculations by Chen et al. (2023), affecting the formation of CH_3SO_3 and $CH_3SO_2O_2$, which are precursors for MSA. Additionally, the rate constant for the reaction of CH_3SO_3 with HO_2, forming MSA, is a factor of 50 smaller in the full mechanism compared to the

https://doi.org/10.5194/egusphere-2026-4710
Preprint. Discussion started: 18 August 2026

Cala mechanism; this reaction is not included in R20 as it was deemed insignificant. These differences result in higher mixing ratios of MSA from the Cala mechanism.

Finally, the similar distributions of HPMTF and DMSO for all three mechanisms are unsurprising; they are species produced from the initial oxidation of DMS (H-abstraction and OH-addition, respectively) and require fewer reactions to represent their formation, unlike MSA or H_2SO_4. However, in our reduced mechanism R20, HPMTF was the sole product of the DMS abstraction pathway, whereas both the reference mechanism and the Cala mechanism include additional reactions of CH_3SCH_2OO, the initial oxidation product. The similar HPMTF distributions across all thousand box models for the five mechanisms demonstrate that these additional reactions are not necessary to represent DMS oxidation in the marine atmosphere, and reinforce the validity of our reduction protocol.

The comparison between the mechanisms demonstrates that our simplified mechanisms are able to reproduce our full reference mechanism, and that the results from our simplified mechanisms differ from a published mechanism used in global modelling (Cala mechanism). The Cala mechanism has been compared to other DMS mechanisms used in global models (Cala et al., 2023; Jongebloed et al., 2025), which found that the production of DMS oxidation products differed between these mechanisms. This work extends that comparison by evaluating the Cala mechanism with an updated, near-explicit mechanism based on chamber studies. Since the formation of gas-phase SO_2, H_2SO_4, OCS, and MSA differed between the Cala mechanism and the full mechanism, we recommend that a simplified mechanism based on that full mechanism (such as R20 or RUKCA) be used in global modelling.

6 Atmospheric implications of the reduced mechanism

The reduced mechanism developed in this study can be applied to global models to improve their modelling of DMS oxidation, without the computational cost of the full near-explicit mechanism. The mechanism produced, with 38 reactions, is of similar size to other global mechanisms that include the HPMTF oxidation pathway, which range from 38–44 reactions (Tashmim et al., 2024; Chen et al., 2023; Cala et al., 2023). Additionally, our evaluation of the reduced mechanism can be used to associate uncertainties with the reduced mechanism from the reduction process.

As identified in Jacob et al. (2026), along with other studies, reactions with gas-phase halogen compounds, such as BrO and Cl, contribute to DMS oxidation (Hoffmann et al., 2016; Chen et al., 2018), however these reactions were omitted from this work as the formation of these species in the troposphere is either not included or underrepresented in the UKCA data used. The reaction of BrO with DMS is an addition reaction, forming DMSO, while the reaction with Cl primarily occurs through the abstraction of a hydrogen atom (Hoffmann et al., 2016). Reactions of BrO and Cl with CH_3SH are abstraction reactions, forming CH_3S. For both DMS and CH_3SH, halogen reactions primarily influence the initial oxidation steps, and subsequent reactions are included in our reduced mechanisms. The following reactions can be added to include halogen-initiated oxidation in the reduced mechanism, using the recommended rate constants from the NASA panel report (Burkholder et al., 2019) and Aranda et al. (2002) (in the case of CH_3SH + BrO) :

$CH_3SH + BrO \rightarrow CH_3S + HOBr$ $\qquad k = 2.2 \times 10^{-15} \times e^{(830/T)}$

https://doi.org/10.5194/egusphere-2026-4710
Preprint. Discussion started: 18 August 2026

$CH_3SH + Cl \rightarrow CH_3S + HCl$ $k = 1.2 \times 10^{-10} \times e^{(150/T)}$

$DMS + BrO \rightarrow DMSO + Br$ $k = 1.4 \times 10^{-14} \times e^{(950/T)}$

$DMS + Cl \rightarrow HPMTF + HCl + OH$ $k = 9.4 \times 10^{-11} \times e^{(190/T)}$

6.1 Incorporation of RUKCA into a global model and comparison with observations

The reduced mechanism (RUKCA) was subsequently implemented in UKCA to improve the representation of marine sulfur chemistry in UKESM. Aerosol and cloud uptake of HPMTF follows the approach of Cala et al. (2023), with the heterogeneous uptake mechanism parameterised after Bauer et al. (2004) and Jacob (2000), and an uptake coefficient of $\gamma = 0.01$ for HPMTF taken from Novak et al. (2021). Two configurations of UKESM (Sellar et al., 2019; Archibald et al., 2020a) were evaluated against airborne measurements of DMS, SO_2, and HPMTF: the mechanism developed in this work, RUKCA, and the standard StratTrop mechanism, a highly simplified four-reaction, three-product scheme employed in CMIP6 studies (Mulcahy et al., 2023; He et al., 2026) that does not include HPMTF. Observations were obtained during the ATom-3 (28 September – 28 October 2017) and ATom-4 (24 April – 21 May 2018) pole-to-pole survey flights over the Pacific and Atlantic Oceans (Wofsy et al., 2018; Thompson et al., 2022). Hourly model output was interpolated onto the flight tracks using the In-Situ Observations Simulator (Russo et al., 2025).

Both configurations overestimated near-surface DMS by more than an order of magnitude (Table 2), indicating that the bias originates upstream of the mechanism change — most plausibly in sea-to-air DMS emissions or boundary-layer mixing, rather than in the gas-phase chemistry. At higher altitudes, interpretation is limited by data availability: ATom-3 reports no DMS

Table 2. Summary of model-observation comparison statistics. N is the total number of paired model outputs and observations, MB is the mean bias, NMB is normalised mean bias, and NMAE is normalised mean absolute error.

	ATom-3					ATom-4				
	DMS		HPMTF	SO_2		DMS		HPMTF	SO_2	
	RUKCA	StratTrop	RUKCA	RUKCA	StratTrop	RUKCA	StratTrop	RUKCA	RUKCA	StratTrop
N	173	173	1076	2000	2000	434	434	725	2404	2404
Obs. mean	6.7	6.7	3.2	21.5	21.5	6.7	6.7	3.8	16.9	16.9
Mod. mean	96.0	83.2	1.4	31.7	35.8	113.8	89.8	1.8	18.7	21.9
Obs. median	4.7	4.7	0.6	13.8	13.8	4.0	4.0	1.1	10.9	10.9
Mod. median	72.3	60.4	0.3	11.5	14.5	86.4	68.5	0.6	8.2	9.8
MB	89.3	76.5	-1.8	9.2	14.3	107.2	83.1	-2.0	1.8	5.0
NMB (%)	1328	1138	-56	43	66	1609	1248	-53	11	30
NMAE (%)	1330	1140	75	132	148	1617	1262	79	108	121

measurements above 3 km (Figure 13), while ATom-4 DMS mixing ratios remain approximately constant at around 4 pptv

https://doi.org/10.5194/egusphere-2026-4710
Preprint. Discussion started: 18 August 2026

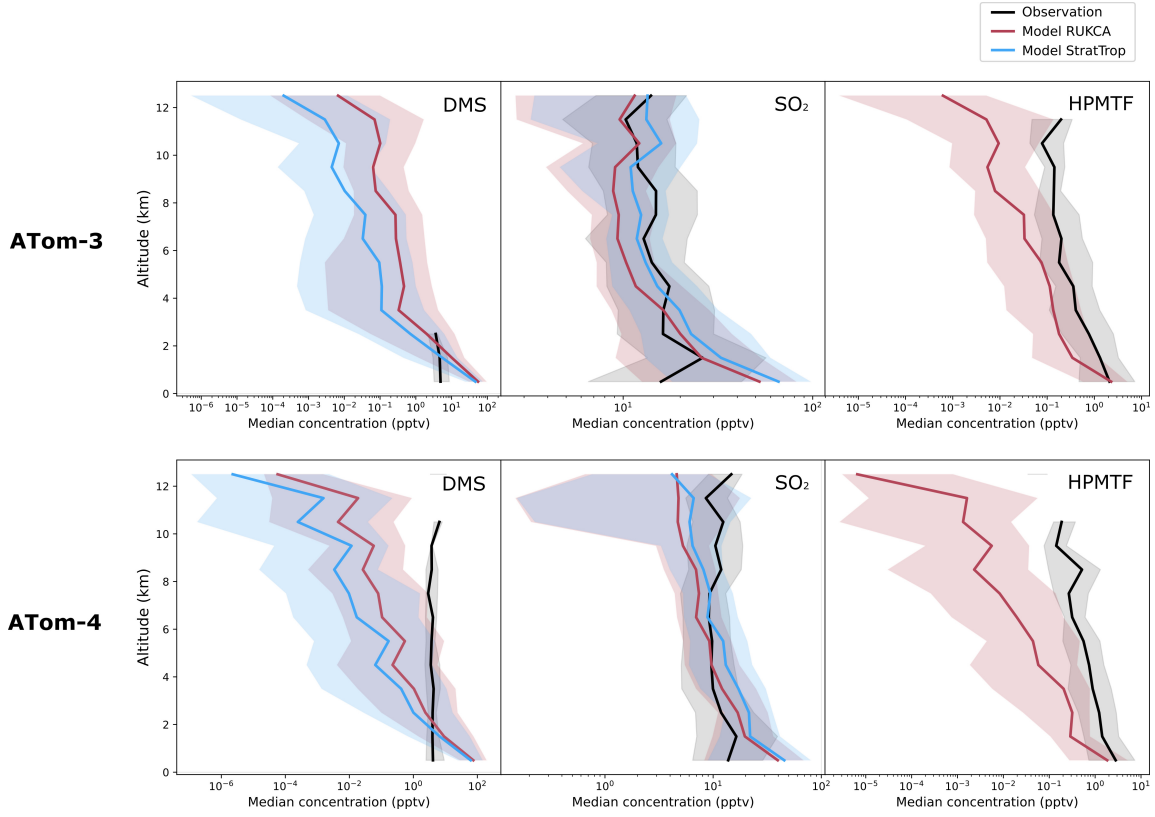

Figure 13. Vertical profiles of modelled and measured DMS, SO_2, and HPMTF concentrations for ATom-3 (first row) and ATom-4 (second row) field campaigns. Median (line) and interquartile range (shading) are shown in 1 km altitude bins.

throughout the profile, in contrast to the modelled decline of several orders of magnitude with height. This invariant profile is more consistent with the detection limit of the Trace Organic Gas Analyzer (TOGA) (Apel et al., 2021) than with a genuine observed distribution.

Agreement was considerably better for SO_2, with RUKCA outperforming StratTrop across most metrics and reducing the normalised mean bias (NMB) from +66% to +43% (ATom-3) and from +30% to +11% (ATom-4). HPMTF, which is present only in RUKCA runs, was reproduced with the smallest normalised mean absolute error (NMAE), despite a persistent low bias of approximately -55%. In fact, a published correction to Veres et al. (2020) reports that subsequent experimental work identified an error in the calibration method used to determine instrument sensitivity for HPMTF during ATom-3 and ATom-4 (Veres et al., 2021); the reported mixing ratios have accordingly been revised downwards by a project-average scaling factor of 0.62 ± 0.11 (1σ). The observations shown here are from the original ATom datasets, as the corrected version is not currently available owing to the NASA Earth science data transition. Applying this correction would reduce the observed HPMTF concentrations by roughly 38%, bringing the modelled values into close agreement with observations. More importantly, the

https://doi.org/10.5194/egusphere-2026-4710
Preprint. Discussion started: 18 August 2026

model captures latitudinal variability well (Figure 14): in ATom-3, modelled HPMTF concentrations are lower in the Southern Hemisphere than in the Northern Hemisphere, consistent with the observed spatial distribution.

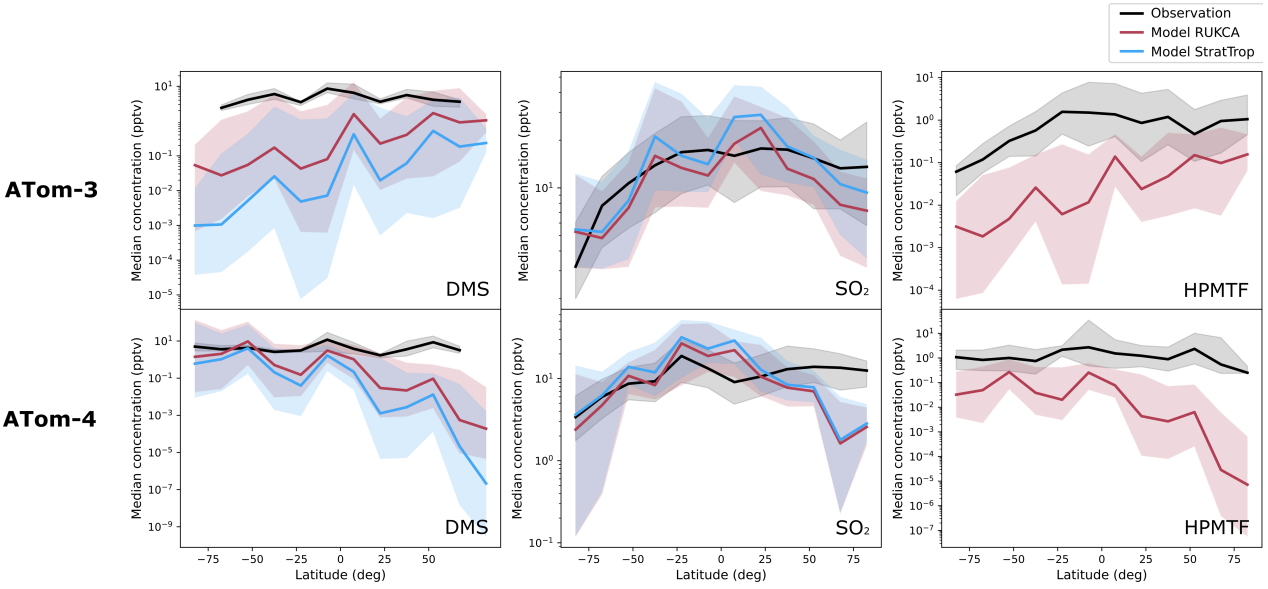

Figure 14. Median concentrations of DMS, SO_2, and HPMTF in 15-degree latitude bands (all altitudes pooled) with interquartile ranges, covering ATom-3 (first row) and ATom-4 (second row) campaigns.

Taken together, these results demonstrate that incorporating the new chemistry into UKESM/UKCA improves the simulation of SO_2 and reproduces the broad distribution of HPMTF at modest computational cost. Relative to the StratTrop configuration, the RUKCA configuration required 3.9% more CPU time and 3.7% more wall-clock time for an one-month integration — equivalent to approximately 51 additional minutes of CPU time and 13 additional minutes of wall-clock time per simulated year under identical processor configurations.

7 Conclusions

This work has built on the work from Jacob et al. (2024) and Jacob et al. (2026), which involved the development and evaluation of a DMS mechanism, through the reduction of the full mechanism (containing 156 reactions) for use in global modelling. Although several mechanisms of different sizes and levels of performance were produced, the smallest mechanism, R20, contained 38 reactions and had an average error of less than 15% for SO_2, MSA, HPMTF, OCS, and H_2SO_4 compared to a comprehensive mechanism. The reduced R20 mechanism was compared to a previously evaluated DMS oxidation mechanism used in global models, which differed in average concentrations of OCS and MSA by factors of 3.6 and 15, respectively. As our mechanism is the only mechanism developed through the reduction of a near-explicit, evaluated DMS oxidation mechanism, which includes recent advances in DMS oxidation pathways, these differences highlight the importance of this work. Our

https://doi.org/10.5194/egusphere-2026-4710
Preprint. Discussion started: 18 August 2026

mechanism is recommended for use in global models; to expand the mechanism and explore gas-phase halogen chemistry, an additional four reactions can be incorporated into the R20 mechanism.

For smaller errors, and a more updated mechanism, the slightly larger RUKCA mechanism (47 reactions) could also be used. Following its implementation in UKCA/UKESM, RUKCA was evaluated against ATom observations and was found to outperform StratTrop (a simplified four-reaction DMS oxidation mechanism) for both SO_2 and HPMTF.

The mechanism developed using a threshold ratio of 1%, R01, had an average error of less than 0.7% for SO_2, MSA, HPMTF, OCS, DMSO and H_2SO_4. Mechanism R01 contained 91 reactions, a 40% reduction compared to the full mechanism, with minimal loss in mechanism performance; as such, it is a near-explicit mechanism suitable for use in modelling fieldwork using box models. The full mechanism is still recommended for chamber studies, which may explore chemical regimes not observed in the marine atmosphere.

The reduction and evaluation of the mechanism were based on randomised box models of the marine boundary layer; this method allowed a large range of marine atmospheres to be explored, which ensured that marine regimes included in global models would be accounted for. This evaluation framework is more robust than a comparison with a few box models or sensitivity tests, and should be used in future reduction work.

The reduced mechanisms developed here provide a traceable link between a near-explicit, experimentally evaluated representation of DMS oxidation, and mechanisms suitable for Earth system models. Their implementation in global models will allow the impact of recent advances in marine sulfur chemistry, including HPMTF and updated MSA and H_2SO_4 formation pathways, to be assessed at the global scale without the computational cost of the full mechanism. If utilised, these reduced mechanisms will provide confidence in the representation of DMS and methanethiol chemistry in global models.

Code and data availability. Equation files for all reduced mechanisms will be made available in Apollo upon publication of this manuscript

Appendix A: Reactions included in mechanism R20

Table A1: The reactions and their rate constants included in the reduced mechanism R20.

	Reaction	Rate constant
1	$CH_3S \rightarrow CH_3SOO$	$1.20 \times 10^{-16} \times e^{(1580/T)} \times [O_2]$
2	$CH_3S + O_3 \rightarrow CH_3SO$	$1.5 \times 10^{-12} \times e^{(360/T)}$
3	$CH_3SH + OH \rightarrow CH_3S$	$9.9 \times 10^{-12} \times e^{(360/T)}$
4	$CH_3SH + NO_3 \rightarrow CH_3S + HNO_3$	$4.4 \times 10^{-13} \times e^{(210/T)}$
5	$CH_3SO + NO_2 \rightarrow CH_3SO_2 + NO$	$1.20 \times 10^{-11} \times 0.75$
6	$CH_3SO + O_3 \rightarrow CH_3O_2 + SO_2$	4.00×10^{-13}
7	$CH_3SO_2 \rightarrow CH_3SO_2O_2$	$1.03 \times 10^{-16} \times e^{(1580/T)} \times [O_2]$

https://doi.org/10.5194/egusphere-2026-4710
Preprint. Discussion started: 18 August 2026

8	$CH_3SO_2 \rightarrow CH_3O_2 + SO_2$	$1.7 \times 10^{15} \times e^{-8.4\times10^3/T} \times e^{1.8\times10^6/T^3}$
9	$CH_3SO_2O_2 + HO_2 \rightarrow CH_3SO_3 + OH$	KAPHO2 $\times$ 0.44
10	$CH_3SO_2O_2 + HO_2 \rightarrow MSA + O_3$	KAPHO2 $\times$ 0.15
11	$CH_3SO_2O_2 + NO \rightarrow CH_3SO_3 + NO_2$	1.00×10^{-11}
12	$CH_3SO_2O_2 \rightarrow CH_3SO_3$	$1.00 \times 10^{-11} \times [RO_2] \times 0.7$
13	$CH_3SO_2O_2 \rightarrow MSA$	$1.00 \times 10^{-11} \times [RO_2] \times 0.3$
14	$CH_3SO_2O_2 \rightarrow CH_3SO_2$	KRSO2O2b
15	$CH_3SO_3 + DMS \rightarrow MSA + HPMTF + OH$	1.45×10^{-13}
16	$CH_3SO_3 \rightarrow CH_3O_2 + SA$	$5.4 \times 10^{12} \times e^{(-9411/T)}$
17	$CH_3SOO \rightarrow CH_3S$	KRSOOb
18	$CH_3SOO \rightarrow CH_3O_2 + SO_2$	KRSOOisom
19	$DMS + OH \rightarrow DMSO + HO_2$	KDMSOH_eq
20	$DMS + NO_3 \rightarrow HPMTF + OH + HNO_3$	$1.9 \times 10^{-13} \times e^{(530/T)}$
21	$DMS + OH \rightarrow HPMTF + OH$	$1.2 \times 10^{-11} \times e^{(-280/T)}$
22	$DMSO + OH \rightarrow MSIA + CH_3O_2$	$6.1 \times 10^{-12} \times e^{(800/T)}$
23	$HOOCH_2S + O_3 \rightarrow SO_2 + HCHO + OH$	$1.5 \times 10^{-12} \times e^{(360/T)}$
24	$HOOCH_2S \rightarrow HOOCH_2SOO$	$1.20 \times 10^{-16} \times e^{(1580/T)} \times [O_2]$
25	$HOOCH_2SOO \rightarrow HOOCH_2S$	KRSOOb
26	$HOOCH_2SOO \rightarrow SO_2 + HCHO + OH$	KRSOOisom
27	$HOOCH_2SOO \rightarrow TPA + HO_2$	$7.13 \times 10^{-31} \times T^{14.02} \times e^{(-2556/T)}$
28	$HPMTF + OH \rightarrow SO_2 + HCHO + OH + CO$	$1.75 \times 10^{-11} \times 0.91$
29	$HPMTF + OH \rightarrow OH + HCHO + OCS$	$1.75 \times 10^{-11} \times 0.09$
30	$HPMTF \rightarrow SO_2 + HCHO + OH + HO_2 + CO$	J("C3H7CHO")
31	$HPMTF \rightarrow HCHO + OCS + HO_2 + OH$	J("CH3OOH")
32	$MSA + OH \rightarrow CH_3SO_3$	2.24×10^{-14}
33	$MSIA + OH \rightarrow CH_3SO_2$	9.00×10^{-11}
34	$OCHSOH + OH \rightarrow OCS + OH$	1.40×10^{-12}
35	$OCHSOH \rightarrow CO + HO_2 + SO_2 + O + HO_2$	J("C3H7CHO")
36	$OCS + OH \rightarrow SO_2 + O + OH$	$7.2 \times 10^{-14} \times e^{(-1070/T)}$
37	$SO_2 + OH \rightarrow HO_2 + SA$	KTER2
38	$TPA + OH \rightarrow OCHSOH + OH$	$5 \times 10^{-11} \times 0.86$

Rate constants: KRSOOb = $1.20\times10^{-16}\times e^{1580/T}/(1.4\times10^{-26}\times e^{4850/T})$, KRSO2O2b = $1.03\times10^{-16}\times e^{1580/T}/(2.35\times10^{-18}\times5.76\times10^{13}\times e^{-8.86\times10^{-2}T})$, KRSOOisom = $7\times10^{14}\times e^{-9659/T}$, KDMSOH_eq = 8.2×10^{-39}[O2]$e^{5376/T}/(1+1.05\times10^{-5}$([O2]/[M])$e^{3644/T})$, KTER2 = (KinfT2 $\times$K0T2$\times$[M])$\times(0.6^{Kb2})$/(KinfT2+K0T2$\times$[M]), KinfT2 = $1.7\times10^{-12}\times(T/298)^{0.2}$, K0T2 = $2.9\times10^{-31}\times(T/298)^{-4.1}$, Kb2 = $(1+(\log_{10}$(K0T2$\times$

https://doi.org/10.5194/egusphere-2026-4710
Preprint. Discussion started: 18 August 2026

[M]/KinfT2))^2)$^{-1}$, J("C3H7CHO") = photolysis rate for n-C_3H_7CHO forming a HCO radical (however, the absorption cross-section calculated for HPMTF could be used instead), KAPHO2 = $5.2 \times 10^{-13} \times e^{980/T}$

Author contributions. YG ran UKCA/UKESM and compared the results to ATom observations. LSDJ ran the box model simulations, produced the reduced mechanisms and performed the evaluations under the supervision of ATA and CG. LSDJ, YG, and ATA wrote the paper. All authors were involved in helpful discussions and contributed to the paper.

Competing interests. Chiara Giorio is a member of the editorial board of Atmospheric Chemistry and Physics.

Acknowledgements. Lorrie S. D. Jacob acknowledges the Cambridge Australia Scholarships and the Cambridge Trust for stipend and tuition support. We also acknowledge the National Environment Research Council (NERC) grant NE/W009412/1.

https://doi.org/10.5194/egusphere-2026-4710
Preprint. Discussion started: 18 August 2026

References

Apel, E., Asher, E., Hills, A., and Hornbrook, R.: ATom: L2 Volatile Organic Compounds (VOCs) from the Trace Organic Gas Analyzer (TOGA), Version 2. ORNL DAAC, Oak Ridge, Tennessee, USA. https://doi.org/10.3334/ORNLDAAC/1936, 2021.

Aranda, A., Diaz de Mera, Y., Rodrı´guez, D., Salgado, S., and Martinez, E.: Kinetic and products of the BrO+CH_3SH reaction: temperature and pressure dependence, Chem. Phys. Lett., 357, 471–476, https://doi.org/https://doi.org/10.1016/S0009-2614(02)00561-4, 2002.

Archibald, A. T., O'Connor, F. M., Abraham, N. L., Archer-Nicholls, S., Chipperfield, M. P., Dalvi, M., Folberth, G. A., Dennison, F., Dhomse, S. S., Griffiths, P. T., Hardacre, C., Hewitt, A. J., Hill, R. S., Johnson, C. E., Keeble, J., Köhler, M. O., Morgenstern, O., Mulcahy, J. P., Ordóñez, C., Pope, R. J., Rumbold, S. T., Russo, M. R., Savage, N. H., Sellar, A., Stringer, M., Turnock, S. T., Wild, O., and Zeng, G.: Description and evaluation of the UKCA stratosphere–troposphere chemistry scheme (StratTrop vn 1.0) implemented in UKESM1, Geosci. Model Dev., 13, 1223–1266, https://doi.org/10.5194/gmd-13-1223-2020, 2020a.

Archibald, A. T., Turnock, S. T., Griffiths, P. T., Cox, T., Derwent, R. G., Knote, C., and Shin, M.: On the changes in surface ozone over the twenty-first century: sensitivity to changes in surface temperature and chemical mechanisms, Philos. Trans. R. Soc., A, 378, 20190 329, https://doi.org/10.1098/rsta.2019.0329, 2020b.

Baalbaki, R., Shen, J., Simon, M., Klebach, H., Ruhl, S., DeVivo, J., Wang, M., Scholz, W., Dada, L., Rörup, B., Stolzenburg, D., Manninen, H. E., Sommer, E., Caudillo-Plath, L., Marie, G., Friedrich, M., Yu, W., Leiminger, M., Alfaouri, D., Amorim, A., Arnoldi-Meadows, T., Beckmann, H., Berntheusel, M., Bräkling, S., Brasseur, Z., Chiu, R., Duplissy, J., Finkenzeller, H., Heinritzi, M., Kunkler, F., Lamkaddam, H., Lopez, B., Mahfouz, N., Makhmutov, V., Martinez, M., Marten, R., Massabo, D., Mauldin, R., Mentler, B., Müller, M., Philippov, M., Piedehierro, A. A., Rato, P., Reinecke, T., Richter, S., Russell, D. M., Schulze, B., Surdu, M., Thakur, R., Tham, Y. J., Tian, P., Tomé, A., Tong, Y., Top, J., Wagner, A. C., Wang, D. S., Wang, Y., Ward, R. X., Weber, S. K., Welti, A., Wu, Y., Zauner-Wieczorek, M., Zhang, J., Curtius, J., Donahue, N. M., El Haddad, I., Flagan, R. C., Hansel, A., Harder, H., Kürten, A., Petäjä, T., Schobesberger, S., Sipilä, M., Volkamer, R., Winkler, P. M., Worsnop, D. R., Christoudias, T., Pozzer, A., Kulmala, M., Kirkby, J., Lehtipalo, K., and He, X.-C.: Role of methanesulfonic acid in atmospheric particle nucleation and growth, Nature, https://doi.org/10.1038/s41586-026-10810-2, 2026.

Bauer, S. E., Balkanski, Y., Schulz, M., Hauglustaine, D. A., and Dentener, F.: Global modeling of heterogeneous chemistry on mineral aerosol surfaces: Influence on tropospheric ozone chemistry and comparison to observations, J. Geophys. Res., 109, D02 304, https://doi.org/10.1029/2003JD003868, 2004.

Beck, L. J., Sarnela, N., Junninen, H., Hoppe, C. J. M., Garmash, O., Bianchi, F., Riva, M., Rose, C., Peräkylä, O., Wimmer, D., Kausiala, O., Jokinen, T., Ahonen, L., Mikkilä, J., Hakala, J., He, X.-C., Kontkanen, J., Wolf, K. K. E., Cappelletti, D., Mazzola, M., Traversi, R., Petroselli, C., Viola, A. P., Vitale, V., Lange, R., Massling, A., Nøjgaard, J. K., Krejci, R., Karlsson, L., Zieger, P., Jang, S., Lee, K., Vakkari, V., Lampilahti, J., Thakur, R. C., Leino, K., Kangasluoma, J., Duplissy, E.-M., Siivola, E., Marbouti, M., Tham, Y. J., Saiz-Lopez, A., Petäjä, T., Ehn, M., Worsnop, D. R., Skov, H., Kulmala, M., Kerminen, V.-M., and Sipilä, M.: Differing mechanisms of new particle formation at two Arctic sites, Geophys. Res. Lett., 48, e2020GL091 334, https://doi.org/https://doi.org/10.1029/2020GL091334, 2021.

Boy, M., Kulmala, M., Ruuskanen, T. M., Pihlatie, M., Reissell, A., Aalto, P. P., Keronen, P., Dal Maso, M., Hellen, H., Hakola, H., Jansson, R., Hanke, M., and Arnold, F.: Sulphuric acid closure and contribution to nucleation mode particle growth, Atmos. Chem. Phys., 5, 863–878, https://doi.org/10.5194/acp-5-863-2005, 2005.

Burkholder, J. B., Sander, S. P., Abbatt, J. P. D., Barker, J. R., Cappa, C., Crounse, J. D., Dibble, T. S., Huie, R. E., Kolb, C. E., Kurylo, M. J., Orkin, V. L., Percival, C. J., Wilmouth, D. M., and Wine, P. H.: Chemical Kinetics and Photochemical Data for Use in Atmospheric Studies, Evaluation No. 19, Tech. rep., JPL Publication 19-5, Jet Propulsion Laboratory, Pasadena, http://jpldataeval.nasa.gov/, 2019.

https://doi.org/10.5194/egusphere-2026-4710
Preprint. Discussion started: 18 August 2026

Cala, B. A., Archer-Nicholls, S., Weber, J., Abraham, N. L., Griffiths, P. T., Jacob, L., Shin, Y. M., Revell, L. E., Woodhouse, M., and Archibald, A. T.: Development, intercomparison and evaluation of an improved mechanism for the oxidation of dimethyl sulfide in the UKCA model, Atmos. Chem. Phys., 23, 14 735–14 760, https://doi.org/10.5194/acp-23-14735-2023, 2023.

Campolongo, F., Cariboni, J., and Saltelli, A.: An effective screening design for sensitivity analysis of large models, Environ. Model. Softw., 22, 1509–1518, https://doi.org/https://doi.org/10.1016/j.envsoft.2006.10.004, 2007.

Chang, Y., Jia, M., Niu, B., Dong, X., and Wang, P.: Reduction of large-scale chemical mechanisms using global sensitivity analysis on reaction class/sub-mechanism, Combust. Flame, 212, 355–366, https://doi.org/10.1016/j.combustflame.2019.11.019, 2020.

Chen, J., Lane, J. R., Bates, K. H., and Kjaergaard, H. G.: Atmospheric gas-phase formation of methanesulfonic acid, Environ. Sci. Technol., 57, 21 168–21 177, https://doi.org/10.1021/acs.est.3c07120, 2023.

Chen, Q., Sherwen, T., Evans, M., and Alexander, B.: DMS oxidation and sulfur aerosol formation in the marine troposphere: a focus on reactive halogen and multiphase chemistry, Atmos. Chem. Phys., 18, 13 617–13 637, https://doi.org/10.5194/acp-18-13617-2018, 2018.

Christensen, N. F., Odai, R., Bates, K. H., and Kjaergaard, H. G.: Calculated absorption cross sections and photolysis rates of hydroperoxyaldehydes, J. Phys. Chem. A, 130, 111–120, https://doi.org/10.1021/acs.jpca.5c06770, 2026.

Covert, D. S., Kapustin, V. N., Quinn, P. K., and Bates, T. S.: New particle formation in the marine boundary layer, J. Geophys. Res. Atmos., 97, 20 581–20 589, https://doi.org/https://doi.org/10.1029/92JD02074, 1992.

Curry, J. A. and Webster, P. J.: Nucleation and diffusional growth, in: Thermodynamics of Atmospheres and Oceans, edited by Holton, J. R., vol. 65, chap. 5, pp. 129–158, Academic Press, Boulder, https://doi.org/10.1016/S0074-6142(99)80027-8, 1999.

Deguillaume, L., Tilgner, A., Schrödner, R., Wolke, R., Chaumerliac, N., and Herrmann, H.: Towards an operational aqueous phase chemistry mechanism for regional chemistry-transport models: CAPRAM-RED and its application to the COSMO-MUSCAT model, J. Atmos. Chem., 64, 1–35, https://doi.org/10.1007/s10874-010-9168-8, 2009.

Ervens, B., George, C., Williams, J. E., Buxton, G. V., Salmon, G. A., Bydder, M., Wilkinson, F., Dentener, F., Mirabel, P., Wolke, R., and Herrmann, H.: CAPRAM 2.4 (MODAC mechanism): an extended and condensed tropospheric aqueous phase mechanism and its application, J. Geophys. Res. Atmos., 108, https://doi.org/https://doi.org/10.1029/2002JD002202, 2003.

Ervens, B., Rickard, A., Aumont, B., Carter, W. P. L., McGillen, M., Mellouki, A., Orlando, J., Picquet-Varrault, B., Seakins, P., Stockwell, W. R., Vereecken, L., and Wallington, T. J.: Opinion: challenges and needs of tropospheric chemical mechanism development, Atmos. Chem. Phys., 24, 13 317–13 339, https://doi.org/10.5194/acp-24-13317-2024, 2024.

Esentürk, E., Abraham, N. L., Archer-Nicholls, S., Mitsakou, C., Griffiths, P., Archibald, A., and Pyle, J.: Quasi-Newton methods for atmospheric chemistry simulations: implementation in UKCA UM vn10.8, Geosci. Model Dev., 11, 3089–3108, https://doi.org/10.5194/gmd-11-3089-2018, 2018.

Fung, K. M., Heald, C. L., Kroll, J. H., Wang, S., Jo, D. S., Gettelman, A., Lu, Z., Liu, X., Zaveri, R. A., Apel, E. C., Blake, D. R., Jimenez, J. L., Campuzano-Jost, P., Veres, P. R., Bates, T. S., Shilling, J. E., and Zawadowicz, M.: Exploring dimethyl sulfide (DMS) oxidation and implications for global aerosol radiative forcing, Atmos. Chem. Phys., 22, 1549–1573, https://doi.org/10.5194/acp-22-1549-2022, 2022.

He, X.-C., Abraham, N. L., Ding, H., Russo, M. R., Grosvenor, D. P., Ge, Y., Wang, X., Jones, A. C., Campuzano-Jost, P., Nault, B., Kupc, A., Blake, D., Jimenez, J. L., Williamson, C. J., Weber, J., Archibald, A. T., , and Gordon, H.: Evaluation of UKESM aerosol size and composition using ATom measurements indicates missing marine aerosol formation mechanisms, Atmos. Chem. Phys., 26, 3805–3851, https://doi.org/10.5194/acp-26-3805-2026, 2026.

https://doi.org/10.5194/egusphere-2026-4710
Preprint. Discussion started: 18 August 2026

Hersbach, H., Bell, B., Berrisford, P., Biavati, G., Horányi, A., Muñoz Sabater, J., Nicolas, J., Peubey, C., Radu, R., Rozum, I., Schepers, D., Simmons, A., Soci, C., Dee, D., and Thépaut, J.-N.: ERA5 hourly data on single levels from 1940 to present, copernicus Climate Change Service (C3S) Climate Data Store (CDS), 30 Oct 2024. 10.24381/cds.adbb2d47, 2023.

Hoffmann, E. H., Tilgner, A., Schrödner, R., Bräuer, P., Wolke, R., and Herrmann, H.: An advanced modeling study on the impacts and atmospheric implications of multiphase dimethyl sulfide chemistry, Proc. Natl. Acad. Sci. U.S.A., 113, 11 776–11 781, https://doi.org/10.1073/pnas.1606320113, 2016.

Hoffmann, E. H., Schrödner, R., Tilgner, A., Wolke, R., and Herrmann, H.: CAPRAM reduction towards an operational multiphase halogen and dimethyl sulfide chemistry treatment in the chemistry transport model COSMO-MUSCAT(5.04e), Geosci. Model Dev., 13, 2587–2609, https://doi.org/10.5194/gmd-13-2587-2020, 2020.

Jacob, D. J.: Heterogeneous chemistry and tropospheric ozone, Atmos. Environ., 34, 2131–2159, https://doi.org/10.1016/S1352-2310(99)00462-8, 2000.

Jacob, L. S. D., Giorio, C., and Archibald, A. T.: Extension, development, and evaluation of the representation of the OH-initiated dimethyl sulfide (DMS) oxidation mechanism in the Master Chemical Mechanism (MCM) v3.3.1 framework, Atmos. Chem. Phys., 24, 3329–3347, https://doi.org/10.5194/acp-24-3329-2024, 2024.

Jacob, L. S. D., Harvey, B. E. H., Giorio, C., and Archibald, A. T.: Determining the key sources of uncertainty in dimethyl sulfide and methanethiol oxidation under tropical, temperate, and polar marine conditions, Atmos. Chem. Phys., 26, 3567–3587, https://doi.org/10.5194/acp-26-3567-2026, 2026.

Jenkin, M. E., Young, J. C., and Rickard, A. R.: The MCM v3.3.1 degradation scheme for isoprene, Atmos. Chem. Phys., 15, 11 433–11 459, https://doi.org/10.5194/acp-15-11433-2015, 2015.

Jenkin, M. E., Khan, M. A., Shallcross, D. E., Bergström, R., Simpson, D., Murphy, K. L., and Rickard, A. R.: The CRI v2.2 reduced degradation scheme for isoprene, Atmos. Environ., 212, 172–182, https://doi.org/10.1016/j.atmosenv.2019.05.055, 2019.

Jongebloed, U. A., Chalif, J. I., Tashmim, L., Porter, W. C., Bates, K. H., Chen, Q., Osterberg, E. C., Koffman, B. G., Cole-Dai, J., Winski, D. A., Ferris, D. G., Kreutz, K. J., Wake, C. P., and Alexander, B.: Dimethyl sulfide chemistry over the industrial era: comparison of key oxidation mechanisms and long-term observations, Atmos. Chem. and Phys., 25, 4083–4106, https://doi.org/10.5194/acp-25-4083-2025, 2025.

Kerminen, V.-M., Chen, X., Vakkari, V., Petäjä, T., Kulmala, M., and Bianchi, F.: Atmospheric new particle formation and growth: review of field observations, Environ. Res. Lett., 13, 103 003, https://doi.org/10.1088/1748-9326/aadf3c, 2018.

Kulmala, M.: How particles nucleate and grow, Science, 302, 1000–1001, https://doi.org/10.1126/science.1090848, 2003.

Lan, X., Thoning, K., and Dlugokencky, E.: Trends in globally-averaged CH4, N2O, and SF6 determined from NOAA Global Monitoring Laboratory measurements, available at: https://doi.org/10.15138/P8XG-AA10 (last access: March 2025), 2025.

Lana, A., Bell, T. G., Simó, R., Vallina, S. M., Ballabrera-Poy, J., Kettle, A. J., Dachs, J., Bopp, L., Saltzman, E. S., Stefels, J., Johnson, J. E., and Liss, P. S.: An updated climatology of surface dimethlysulfide concentrations and emission fluxes in the global ocean, Global Biogeochem. Cycles, 25, GB1004, https://doi.org/10.1029/2010GB003850, 2011.

Mann, G. W., Carslaw, K. S., Spracklen, D. V., Ridley, D. A., Manktelow, P. T., Chipperfield, M. P., Pickering, S. J., and Johnson, C. E.: Description and evaluation of GLOMAP-mode: a modal global aerosol microphysics model for the UKCA composition-climate model, Geosci. Model Dev., 3, 519–551, https://doi.org/10.5194/gmd-3-519-2010, 2010.

https://doi.org/10.5194/egusphere-2026-4710
Preprint. Discussion started: 18 August 2026

Mauersberger, G.: ISSA (iterative screening and structure analysis)—a new reduction method and its application to the tropospheric cloud chemical mechanism RACM/CAPRAM2.4, Atmos. Environ., 39, 4341–4350, https://doi.org/https://doi.org/10.1016/j.atmosenv.2005.02.015, 2005.

Mulcahy, J. P., Jones, C. G., Rumbold, S. T., Kuhlbrodt, T., Dittus, A. J., Blockley, E. W., Yool, A., Walton, J., Hardacre, C., Andrews, T., Bodas-Salcedo, A., Stringer, M., de Mora, L., Harris, P., Hill, R., Kelley, D., Robertson, E., , and Tang, Y.: UKESM1.1: development and evaluation of an updated configuration of the UK Earth System Model, Geosci. Model Dev., 16, 1569–1600, https://doi.org/10.5194/gmd-16-1569-2023, 2023.

Novak, G., Fite, C., Holmes, C., Veres, P., Neuman, J., Faloona, I., Thornton, J., Wolfe, G., Vermeuel, M., Jernigan, C., Peischl, J., Ryerson, T., Thompson, C., Bourgeois, I., Warneke, C., Gkatzelis, G., Coggon, M., Sekimoto, K., Bui, T., Dean-Day, J., Diskin, G., DiGangi, J., Nowak, J., Moore, R., Wiggins, E., Winstead, E., Robinson, C., Thornhill, K., Sanchez, K., Hall, S., Ullmann, K., Dollner, M., Weinzierl, B., Blake, D., and Bertram, T.: Rapid cloud removal of dimethyl sulfide oxidation products limits SO_2 and cloud condensation nuclei production in the marine atmosphere, Proc. Natl. Acad. Sci. U.S.A., 118, e2110472 118, https://doi.org/10.1073/pnas.2110472118, 2021.

Russo, M. R., Bartholomew, S. L., Hassell, D., Mason, A. M., Neininger, E., Perman, A. J., Sproson, D. A. J., Watson-Parris, D., and Abraham, N. L.: Virtual Integration of Satellite and In-Situ Observation Networks (VISION) v1.0: In-Situ Observations simulator (ISO_simulator), Geosci. Model Dev., 18, 181–191, https://doi.org/10.5194/gmd-18-181-2025, 2025.

Seinfeld, J. H. and Pandis, S. N.: Atmospheric trace constituents, in: Atmospheric Chemistry and Physics, from Air Pollution to Climate Change, pp. 18–65, Wiley, New York, USA, 2006.

Sellar, A. A., Jones, C. G., Mulcahy, J. P., Tang, Y., Yool, A., Wiltshire, A., O'Connor, F. M., Stringer, M., Hill, R., Palmieri, J., Woodward, S., de Mora, L., Kuhlbrodt, T., Rumbold, S. T., Kelley, D. I., Ellis, R., Johnson, C. E., Walton, J., Abraham, N. L., Andrews, M. B., Andrews, T., Archibald, A. T., Berthou, S., Burke, E., Blockley, E., Carslaw, K., Dalvi, M., Edwards, J., Folberth, G. A., Gedney, N., Griffiths, P. T., Harper, A. B., Hendry, M. A., Hewitt, A. J., Johnson, B., Jones, A., Jones, C. D., Keeble, J., Liddicoat, S., Morgenstern, O., Parker, R. J., Predoi, V., Robertson, E., Siahaan, A., Smith, R. S., Swaminathan, R., Woodhouse, M. T., Zeng, G., and Zerroukat, M.: UKESM1: Description and evaluation of the U.K. Earth System Model, J. Adv. Model. Earth Syst., 11, 4513–4558, https://doi.org/10.1029/2019MS001739, 2019.

Squire, O. J., Archibald, A. T., Griffiths, P. T., Jenkin, M. E., Smith, D., and Pyle, J. A.: Influence of isoprene chemical mechanism on modelled changes in tropospheric ozone due to climate and land use over the 21st century, Atmos. Chem. Phys., 15, 5123–5143, https://doi.org/10.5194/acp-15-5123-2015, 2015.

Stein, B. V., Raponi, E., Sadeghi, Z., Bouman, N., Van Ham, R. C. H. J., and Bäck, T.: A comparison of global sensitivity analysis methods for explainable AI with an application in genomic prediction, IEEE Access, 10, 103 364–103 381, https://doi.org/10.1109/ACCESS.2022.3210175, 2022.

Szopa, S., Naik, V., Adhikary, B., Artaxo, P., Berntsen, T., Collins, W., Fuzzi, S., Gallardo, L., Kiendler-Scharr, A., Klimont, Z., Liao, H., Unger, N., and Zanis, P.: Short-Lived Climate Forcers, in: Climate Change 2021: The Physical Science Basis. Contribution of Working Group I to the Sixth Assessment Report of the Intergovernmental Panel on Climate Change, edited by Masson-Delmotte, V., Zhai, P., Pirani, A., Connors, S., Péan, C., Berger, S., Caud, N., Chen, Y., Goldfarb, L., Gomis, M., Huang, M., Leitzell, K., Lonnoy, E., Matthews, J., Maycock, T., Waterfield, T., Yelekçi, O., Yu, R., and Zhou, B., chap. 6, p. 817–922, Cambridge University Press, Cambridge, United Kingdom and New York, NY, USA, https://doi.org/10.1017/9781009157896.008, 2021.

https://doi.org/10.5194/egusphere-2026-4710
Preprint. Discussion started: 18 August 2026

Tashmim, L., Porter, W. C., Chen, Q., Alexander, B., Fite, C. H., Holmes, C. D., Pierce, J. R., Croft, B., and Ishino, S.: Contribution of expanded marine sulfur chemistry to the seasonal variability of dimethyl sulfide oxidation products and size-resolved sulfate aerosol, Atmos. Chem. Phys., 24, 3379–3403, https://doi.org/10.5194/acp-24-3379-2024, 2024.

Thompson, C. R., Wofsy, S. C., Prather, M. J., Newman, P. A., Hanisco, T. F., Ryerson, T. B., Fahey, D. W., Apel, E. C., Brock, C. A., Brune, W. H., Froyd, K., Katich, J. M., Nicely, J. M., Peischl, J., Ray, E., Veres, P. R., Wang, S., Allen, H. M., Asher, E., Bian, H., Blake, D., Bourgeois, I., Budney, J., Bui, T. P., Butler, A., Campuzano-Jost, P., Chang, C., Chin, M., Commane, R., Correa, G., Crounse, J. D., Daube, B., Dibb, J. E., DiGangi, J. P., Diskin, G. S., Dollner, M., Elkins, J. W., Fiore, A. M., Flynn, C. M., Guo, H., Hall, S. R., Hannun, R. A., Hills, A., Hintsa, E. J., Hodzic, A., Hornbrook, R. S., Huey, L. G., Jimenez, J. L., Keeling, R. F., Kim, M. J., Kupc, A., Lacey, F., Lait, L. R., Lamarque, J.-F., Liu, J., McKain, K., Meinardi, S., Miller, D. O., Montzka, S. A., Moore, F. L., Morgan, E. J., Murphy, D. M., Murray, L. T., Nault, B. A., Neuman, J. A., Nguyen, L., Gonzalez, Y., Rollins, A., Rosenlof, K., Sargent, M., Schill, G., Schwarz, J. P., Clair, J. M. S., Steenrod, S. D., Stephens, B. B., Strahan, S. E., Strode, S. A., Sweeney, C., Thames, A. B., Ullmann, K., Wagner, N., Weber, R., Weinzierl, B., Wennberg, P. O., Williamson, C. J., Wolfe, G. M., and Zeng, L.: The NASA Atmospheric Tomography (ATom) mission: imaging the chemistry of the global atmosphere, Bull. Am. Meteorol. Soc., 103, E761–E790, https://doi.org/10.1175/BAMS-D-20-0315.1, 2022.

Veres, P. R., Andrew Neuman, J., Bertram, T. H., Assaf, E., Wolfe, G. M., Williamson, C. J., Weinzierl, B., Tilmes, S., Thompson, C. R., Thames, A. B., Schroder, J. C., Saiz-Lopez, A., Rollins, A. W., Roberts, J. M., Price, D., Peischl, J., Nault, B. A., Møller, K. H., Miller, D. O., Meinardi, S., Li, Q., Lamarque, J. F., Kupc, A., Kjaergaard, H. G., Kinnison, D., Jimenez, J. L., Jernigan, C. M., Hornbrook, R. S., Hills, A., Dollner, M., Day, D. A., Cuevas, C. A., Campuzano-Jost, P., Burkholder, J., Paul Bui, T., Brune, W. H., Brown, S. S., Brock, C. A., Bourgeois, I., Blake, D. R., Apel, E. C., and Ryerson, T. B.: Global airborne sampling reveals a previously unobserved dimethyl sulfide oxidation mechanism in the marine atmosphere, Proc. Natl. Acad. Sci. U.S.A., 117, 4505–4510, https://doi.org/10.1073/pnas.1919344117, 2020.

Veres, P. R., Andrew Neuman, J., Bertram, T. H., Assaf, E., Wolfe, G. M., Williamson, C. J., Weinzierl, B., Tilmes, S., Thompson, C. R., Thames, A. B., Schroder, J. C., Saiz-Lopez, A., Rollins, A. W., Roberts, J. M., Price, D., Peischl, J., Nault, B. A., Møller, K. H., Miller, D. O., Meinardi, S., Li, Q., Lamarque, J. F., Kupc, A., Kjaergaard, H. G., Kinnison, D., Jimenez, J. L., Jernigan, C. M., Hornbrook, R. S., Hills, A., Dollner, M., Day, D. A., Cuevas, C. A., Campuzano-Jost, P., Burkholder, J., Paul Bui, T., Brune, W. H., Brown, S. S., Brock, C. A., Bourgeois, I., Blake, D. R., Apel, E. C., and Ryerson, T. B.: Correction for Veres et al., Global airborne sampling reveals a previously unobserved dimethyl sulfide oxidation mechanism in the marine atmosphere, Proc. Natl. Acad. Sci. U.S.A., 118, e2113268 118, https://doi.org/10.1073/pnas.2113268118, 2021.

Walters, D., Baran, A. J., Boutle, I., Brooks, M., Earnshaw, P., Edwards, J., Furtado, K., Hill, P., Lock, A., Manners, J., Morcrette, C., Mulcahy, J., Sanchez, C., Smith, C., Stratton, R., Tennant, W., Tomassini, L., Van Weverberg, K., Vosper, S., Willett, M., Browse, J., Bushell, A., Carslaw, K., Dalvi, M., Essery, R., Gedney, N., Hardiman, S., Johnson, B., Johnson, C., Jones, A., Jones, C., Mann, G., Milton, S., Rumbold, H., Sellar, A., Ujiie, M., Whitall, M., Williams, K., and Zerroukat, M.: The Met Office Unified Model Global Atmosphere 7.0/7.1 and JULES Global Land 7.0 configurations, Geosci. Model Dev., 12, 1909–1963, https://doi.org/https://doi.org/10.5194/gmd-12-1909-2019, 2019.

Wang, Z., Couvidat, F., and Sartelet, K.: GENerator of reduced Organic Aerosol mechanism (GENOA v1.0): an automatic generation tool of semi-explicit mechanisms, Geosci. Model Dev., 15, 8957–8982, https://doi.org/10.5194/gmd-15-8957-2022, 2022.

Weisstein, E. W.: Sphere point picking, from MathWorld–a Wolfram Web resource, available at: https://mathworld.wolfram.com/SpherePointPicking.html (last access: Feb 2025), 2002.

https://doi.org/10.5194/egusphere-2026-4710
Preprint. Discussion started: 18 August 2026

Wiser, F., Place, B. K., Sen, S., Pye, H. O. T., Yang, B., Westervelt, D. M., Henze, D. K., Fiore, A. M., and McNeill, V. F.: AMORE-Isoprene v1.0: a new reduced mechanism for gas-phase isoprene oxidation, Geosci. Model Dev., 16, 1801–1821, https://doi.org/10.5194/gmd-16-1801-2023, 2023.

Wofsy, S., Afshar, S., Allen, H., Apel, E., Asher, E., Barletta, B., Bent, J., Bian, H., Biggs, B., Blake, D., Blake, N., Bourgeois, I., Brock, C., Brune, W., Budney, J., Bui, T., Butler, A., Campuzano-Jost, P., Chang, C., Chin, M., Commane, R., Correa, G., Crounse, J., Cullis, P. D., Daube, B., Day, D., Dean-Day, J., Dibb, J., DiGangi, J., Diskin, G., Dollner, M., Elkins, J., Erdesz, F., Fiore, A., Flynn, C., Froyd, K., Gesler, D., Hall, S., Hanisco, T., Hannun, R., Hills, A., Hintsa, E., Hoffman, A., Hornbrook, R., Huey, L., Hughes, S., Jimenez, J., Johnson, B., Katich, J., Keeling, R., Kim, M., Kupc, A., Lait, L., Lamarque, J.-F., Liu, J., McKain, K., Mclaughlin, R., Meinardi, S., Miller, D., Montzka, S., Moore, F., Morgan, E., Murphy, D., Murray, L., Nault, B., Neuman, J., Newman, P., Nicely, J., Pan, X., Paplawsky, W., Peischl, J., Prather, M., Price, D., Ray, E., Reeves, J., Richardson, M., Rollins, A., Rosenlof, K., Ryerson, T., Scheuer, E., Schill, G., Schroder, J., Schwarz, J., St.Clair, J., Steenrod, S., Stephens, B., Strode, S., Sweeney, C., Tanner, D., Teng, A., Thames, A., Thompson, C., Ullmann, K., Veres, P., Vieznor, N., Wagner, N., Watt, A., Weber, R., Weinzierl, B., Wennberg, P., Williamson, C., Wilson, J., Wolfe, G., Woods, C., and Zeng, L.: ATom: merged atmospheric chemistry, trace gases, and aerosols, https://doi.org/10.3334/ORNLDAAC/1581, ORNL Distributed Active Archive Center, Date Accessed: 2026-07-24, 2018.

Wohl, C., Villamayor, J., Galí, M., Mahajan, A. S., Fernández, R. P., Cuevas, C. A., Bossolasco, A., Li, Q., Kettle, A. J., Williams, T., Sarda-Esteve, R., Gros, V., Simó, R., and Saiz-Lopez, A.: Marine emissions of methanethiol increase aerosol cooling in the Southern Ocean, Sci. Adv., 10, eadq2465, https://doi.org/10.1126/sciadv.adq2465, 2024.